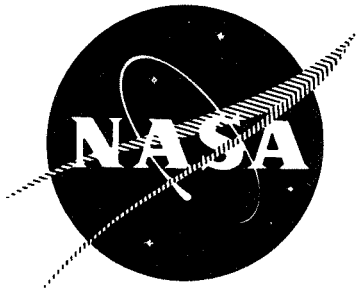

NASA CR-72625
R-8076

ANALYSIS OF THE ACOUSTIC BEHAVIOR OF BAFFLED COMBUSTION CHAMBERS

by

C. L. Oberg, T. L. Wong, and R. A. Schmeltzer

Rocketdyne
A Division of North American Rockwell Corporation

prepared for

NATIONAL AERONAUTICS AND SPACE ADMINISTRATION

NASA Lewis Research Center
Contract NAS 3-11226

Dr. R. J. Priem, Project Manager

NOTICE

This report was prepared as an account of Government-sponsored work. Neither the United States, nor the National Aeronautics and Space Administration (NASA), nor any person acting on behalf of NASA:

A. Makes any warranty or representation, expressed or implied, with respect to the accuracy, completeness, or usefulness of the information contained in this report, or that the use of any information, apparatus, method, or process disclosed in this report may not infringe privately owned rights; or

B. Assumes any liabilities with respect to the use of, or for damages resulting from the use of, any information, apparatus, method or process disclosed in this report.

As used above, "person acting on behalf of NASA" includes any employee or contractor of NASA, or employee of such contractor, to the extent that such employee or contractor of NASA or employee of such contractor prepares, disseminates, or provides access to any information pursuant to his employment or contract with NASA, or his employment with such contractor.

NASA CR-72625
R-8076

FINAL REPORT

ANALYSIS OF THE ACOUSTIC BEHAVIOR OF BAFFLED COMBUSTION CHAMBERS

BY

C. L. Oberg, T. L. Wong, and R. A. Schmeltzer

prepared for

NATIONAL AERONAUTICS AND SPACE ADMINISTRATION

January 1970

CONTRACT NAS 3-11226

NASA Lewis Research Center
Cleveland, Ohio

Dr. R. J. Priem, Project Manager

FOREWORD

The research program described herein was sponsored by the National Aeronautics and Space Administration, Lewis Research Center, Cleveland, Ohio, 44135, under contract NAS3-11226. The study was conducted during the 14-month period beginning 22 May 1968 and ending 22 July 1969. NASA Project Manager was Dr. R. J. Priem. The Rocketdyne program manager was Mr. T. A. Coultas, with Dr. C. L. Oberg as responsible engineer.

Dr. Oberg was largely responsible for formulation of the variational-iterational technique; Dr. T. L. Wong was responsible for numerical solution of the resultant equations, and Dr. R. A. Schmeltzer developed the secular equation method.

This report has been assigned the Rocketdyne report No. R-8076.

ABSTRACT

As a means of studying the effects of baffles on acoustic modes of combustion instability, analytical methods have been developed for calculating the wave motion in closed, baffled chambers with rigid or nonrigid boundaries. These methods encompass solving the wave equation for the baffled chamber by converting the differential equation and boundary conditions to an integral equation which, in turn, is solved by approximate means. A variational technique in combination with an iterated approximation was used to solve the integral equation. Numerical results were obtained for two-dimensional chambers containing one or several equal length and equally spaced baffles. The results show an essentially continuous pressure distribution along the baffle tips. Requirements for continuity of velocity and energy flux are automatically met with this method. Furthermore, the effects of a single baffle on the stability of a chamber with nonrigid walls, i.e., gain/loss-type boundary conditions, has been successfully analyzed for one particular two-dimensional geometry. Thus, the ability to generalize the method for nonzero boundary conditions has also been demonstrated. Finally, convergence of the iteration scheme has not been proved but very good numerical results were obtained and it is likely that adequate convergence can be achieved.

CONTENTS

ILLUSTRATIONS

NOMENCLATURE

$a_{\mu q}^{(n)}$ = coefficient defined by Eq. 12 ($lb_f/in.^3$)

A = variational parameter

$A_{\mu qm}$ = defined by Eq. 9 ($lb_f/in.^3$)

c = sound velocity, in./sec

$G_a(\vec{r}|\vec{r}_0)$ = Green's function for main chamber

$G_{b\mu}(\vec{r}|\vec{r}_0)$ = Green's function for μ^{th} baffle compartment

j = $(-1)^{1/2}$

k = ω/c, $inch^{-1}$

k_q = $(k^2 - q^2\pi^2/w^2)^{1/2}$, $inch^{-1}$

k_m = $(k^2 - m^2\pi^2/W^2)^{1/2}$, $inch^{-1}$

ℓ = baffle length, inches

L = main chamber length, inches

L_t = $(\ell + L)$, total chamber length, inches

m = index, positive integral values

$\vec{N}$ = unit normal vector directed outward

p = pressure, $lb_f/in.^2$

q = index, positive integral values

$\vec{r}$ = position vector, inches

S = surface area, sq in.

S_t = total chamber-compartment interface area, sq in.

S_μ = chamber-compartment interface area of μ^{th} compartment, sq in.

u = longitudinal velocity component, in./sec

V = chamber volume, $inch^3$

w = width of baffle compartment, inches

W = width of main chamber, inches

x = longitudinal position coordinate, inches

y = transverse position coordinate, inches

y_I = specific acoustic admittance of injector end (dimensionless)

y_N = specific acoustic admittance of nozzle end (dimensionless)

ε_ν = 1 if $\nu = 0$, 2 if $\nu \neq 0$

η = eigenvalue for reference volume, $inch^{-1}$

Λ_n = $\{\int \phi_n^2 \, dV\}/V$, dimensionless

μ = baffle compartment index, positive integral values

ξ = normal pressure gradient, $lb_f/in.$

ρ = time averaged gas density, $lb_m/in.^3$

ϕ = $\omega W/c$

$\phi_n(\vec{r})$ = eigenfunctions for reference volume

ω = angular frequency, radians/sec

SUBSCRIPTS

a = refers to main chamber

b = refers to baffle compartments

μ = refers to μ^{th} baffle compartment

0 = refers to source coordinates for Green's functions

SUPERSCRIPTS

s = refers to source surface (interface)

overbar = denotes particular index

(n) = refers to n^{th} iteration

$\wedge$ = denotes maximum value retained in summation

SUMMARY

Analytical methods have been developed for calculating the wave motion in closed, baffled chambers with rigid and nonrigid boundaries. Application of these methods to the design of injector-face baffles in liquid-propellant engines will provide significant insight into the effects of baffles on combustion stability.

During this program, approximate solutions to the wave equation, with essentially continuous pressure distributions, were obtained for closed, two-dimensional chambers containing an unrestricted number of equal length and equally spaced baffles. Solutions were obtained by converting the wave equation and boundary conditions to an integral equation; this integral equation was solved with a combination of variation and iteration methods. The mathematical techniques used to obtain these solutions apply equally well to cylindrical or annular chambers, and to unequal baffle lengths or spacing, although with some increase in complexity. As yet, however, numerical results have not been obtained for these more complicated configurations. The calculated frequencies and oscillatory pressure distributions for two-dimensional chambers are in good agreement with data obtained from bench-scale acoustic models.

Calculations were also made for similar chambers with a loss-type boundary condition (admittance) at the nozzle end of the chamber, and a gain-type boundary condition at the injector end. These boundary conditions simulate pressure-coupled gains and losses. Results for the particular case considered suggest that baffles improve stability in an engine by reducing velocity rather than pressure coupling. This indication is drawn from the fact that, in the pressure-coupled (acoustic-admittance) case considered, the addition of one baffle was found to worsen rather than improve stability. Nevertheless, the ability to employ the analytical approach with nonzero boundary conditions has been demonstrated.

Convergence of the iteration scheme has not been proved, but very good numerical results were obtained. It appears likely that adequate convergence can be achieved.

INTRODUCTION

Baffles are typically comprised of an array of blades, often straight, mounted on the injector face and projecting several inches downstream. Typical configurations may be found in Ref. 1 and 2.

Currently, baffles are designed principally from consideration of the oscillatory velocity characteristics of observed or anticipated acoustic modes for the chamber. The baffle blades are generally positioned at or near the calculated location of the velocity antinodes (maxima); the antinodal locations are calculated from acoustic expressions that pertain to closed, unbaffled chambers. Thus located, the baffles are thought to "interfere" with the normal acoustic modes and thereby promote stability. Although this approach is often successfully applied, it is unsatisfactory because no consideration is given to the wave motion possible once the baffles are installed.

Further, empirical design rules have been developed from motor firing and some acoustic modeling results, but these, too, are unsatisfactory because they lack quantitative character and are not always valid. Moreover, these results provide little insight into the manner in which stability is improved. Several of these techniques are described in Ref. 1 and 2.

It is evident that a better fundamental understanding of the oscillatory characteristics of baffled chambers would contribute significantly to more nearly sound design techniques. Few previous analyses of these oscillatory characteristics have been reported, perhaps because of the mathematical difficulties involved. One approximation used is obtained by first assuming the wave motion within the baffle compartments is only longitudinal, and then matching the ratio of pressure and normal component of velocity (admittance) at the interface between the compartments and the main chamber. This approximation yields a moderately good estimate of the frequency depression produced by baffles at the normal chamber frequencies.

However, in this approximation, none of the continuity requirements on pressure, velocity, and energy flux across the interface are met. Further, baffle spacing does not enter into the calculation. Therefore, this approximation is lacking in many respects.

Other attempts at analysis of the problem have been largely unsuccessful. Therefore, these provide little foundation on which to base another study. Fortunately, however, thorough analyses have been developed in the acoustics literature for related kinds of problems. These do provide a satisfactory starting point for an analysis of baffled chambers.

ANALYTICAL APPROACH

The analytical approach is based on the assumption that the linear acoustic behavior of a baffled chamber adequately approximates the wave motion in a baffled combustion chamber. Although this approximation may be lacking in some respects, it has been effectively used for stability problems in the past, and further it is certainly an appropriate starting point for more thorough analysis.

Thus, the effects of baffles were investigated by solving the wave equation for closed, baffled cavities. The effects of combustion driving and the various loss processes were simulated to some extent by employing gain/loss-type boundary conditions. The effects of steady flow have been largely neglected; however, a modified ("virtual") boundary condition was employed, which partially accounts for this flow.

Although the problem has been simplified to the extent that only the wave equation need be solved, the solution is still not straightforward. The presence of baffles (the boundary shape) precludes the use of the separation-of-variables technique to solve this equation. For similar problems Morse (Ref. 3, pg. 1039) suggests using an integral formulation of the problem and then solving the resultant integral equation by approximate means.

Accordingly, the wave equation and boundary conditions were rewritten as an integral equation, which was solved by two approximate means: an iteration-variation technique and a secular determinant technique. Satisfactory results were only obtained with the former method.

The approximations were guided by, and tested against, frequency and oscillatory-pressure data from bench-scale acoustic modeling tests. It is clear from these data that the normal transverse modes of the chamber are distorted, but not eliminated, by the addition of baffles. Further, the baffle compartments and main chamber generally act as a closely coupled oscillatory system with a continuous pressure distribution near the interface between them. However, compartment modes, which are largely confined to the baffle compartments, also appear. These observations from modeling tests are compatible with engine test (hot-firing) data as well.

ANALYSIS

INTEGRAL FORMULATION

Because the wave equation cannot be solved by separation of variables for the baffled chamber, this equation and the accompanying boundary conditions were converted to an integral equation that was solved by approximate means. The steps involved in this conversion are described by Morse (Ref. 4, page 321); the Helmholtz equation, which is the wave equation for a harmonic time dependence

$$\nabla^2 p + k^2 p = 0 \tag{1}$$

may be rewritten as

$$p(\vec{r}) = \int_S G(\vec{r}|\vec{r}_0)\ \vec{N}\cdot\nabla_0\ p(\vec{r}_0)\ dS_0 \tag{2}$$

where $G(\vec{r}|\vec{r}_0)$ is a Green's function, which satisfies either the same boundary conditions as the pressure (p), or a zero-gradient boundary condition. In addition, Green's function satisfies the differential equation

$$\nabla^2 G + k^2 G = -\delta(\vec{r} - \vec{r}_0) \tag{3}$$

where $\delta(\vec{r} - \vec{r}_0)$ is a Dirac delta function.

The integral expression for pressure is used with separate Green's functions written for each baffle compartment and also for the main chamber. Each of these Green's functions is zero outside of the compartment to which it applies. However, the oscillatory pressure and normal component of velocity must be continuous across the interface between each region. Therefore, at this interface,

$$p_a(\vec{r}_s) = \int_S G_a(\vec{r}_s|\vec{r}_0)\ \xi(\vec{r}_0)dS_0 = -\int_S G_{b\mu}(\vec{r}_s|\vec{r}_0)\ \xi(\vec{r}_0)dS_0 = p_{b\mu}(\vec{r}_s) \tag{4}$$

where $G_a(\vec{r}|\vec{r}_0)$ is the Green's function for the main chamber, $G_{b\mu}(\vec{r}|\vec{r}_0)$ is the Green's function for the μ^{th} baffle compartment, and

$$\xi(\vec{r}_0^s) = \vec{N}\cdot\nabla\, p_a(\vec{r}_0^s) \qquad (5)$$

$$= -\vec{N}\cdot\nabla\, p_b(\vec{r}_0^s)$$

Assuming the baffle compartments and main chamber have regular geometries, the necessary Green's functions can be readily developed. If the set of equations indicated by Eq. 4 are solved for ξ, then the pressure at any point within the combustion chamber can be calculated from Eq. 2. In addition, a set of frequencies (eigenvalues) will be obtained from Eq. 4.

Morse (Ref. 4, pg. 680) suggests approximate solution of Eq. 4 by a variational technique; he also suggests a secular-equation technique for similar problems (Ref. 3, pg. 1040). From each of these methods, a characteristic equation is obtained which, in turn, must be solved for the eigenvalues or frequencies of the chamber.

The variational-iterational technique will be described in some detail. A description of the secular-equation method will be given in Appendix A because no satisfactory results were obtained with this method.

VARIATION-ITERATION TECHNIQUE

Morse (Ref. 4, pg. 680) developed a variational function from Eq. 4, although he was considering only two coupled cavities. An approximate expression for ξ, or rather the normal velocity, containing an unspecified parameter was inserted into the variational function and the variational procedure was used to optimize the parameter, i.e., select the "best" value. From this, a second-order estimate of the eigenvalue (frequency) and a first-order estimate of the eigenfunction (pressure) was obtained.

If this procedure is applied to the baffle problem with an approximate function of the form $\xi = A\,\overline{\xi}$ being used, where A is the variational parameter but $\overline{\xi}$ is a still unspecified function of position, the variational procedure leads to the result

$$\int_S \overline{\xi}(p_a - p_b)\, dS = 0 \tag{6}$$

where

$$p_a = \overline{A}\int_S G_a(\vec{r}_s|\vec{r}_0)\ \overline{\xi}(\vec{r}_0)\ dS$$

$$p_b = -\overline{A}\int_S G_b(\vec{r}_s|\vec{r}_0)\ \overline{\xi}(\vec{r}_0)\ dS$$

The mathematical details concerning the development of Eq. 6 are summarized in Appendix A. Because $\overline{\xi}$ is proportional to the normal component of velocity, this procedure shows that the best approximate eigenvalue (frequency) is obtained by requiring continuity of the energy flux at the interface between the main chamber and the baffle compartments. Continuity of the normal velocity is automatically satisfied but pressure is not, unless the exact solution is used.

During the initial part of this program, several approximations were tried for $\overline{\xi}$. (The overbar on ξ will be subsequently omitted because the distinction is unimportant.) However, in each case, the pressure match across the interface was poor. Consequently, an iteration procedure was devised to improve these initial estimates.

The iteration was done with the aid of orthogonality properties. Green's functions were obtained as expansions in terms of orthogonal functions, and similar kinds of expansions were obtained for the pressures. The iteration was done by: (1) initially assuming a pressure distribution

on the baffle-compartment side of the interface; (2) calculating the corresponding normal gradient (ξ) from the expansion;(3) then calculating the pressure on the chamber side from that expansion for ξ; and (4) finally equating expansions for p_a and p_b to obtain a new set of coefficients for p_b and complete the cycle.

Convergence of this iteration scheme was not proved; however, good numerical results were obtained.

GAIN/LOSS-TYPE BOUNDARY CONDITIONS

Nonzero, admittance-type boundary conditions can be added at each end of the chamber without difficulty. By defining Green's functions, which satisfy the same boundary conditions at the closed ends of the chamber as those satisfied by the pressure, the foregoing equations may be used without change.

ANALYTICAL RESULTS

TWO-DIMENSIONAL CHAMBER WITH RIGID WALLS

With the variational method, continuity of the normal component of velocity and energy flux across the interface between the main chamber and baffle compartments is automatically satisfied. However, continuity of pressure is not satisfied unless the exact solution is found. This interface, as sketched below, is, of course, simply a convenient surface on which to match solutions for the compartment and main chamber.

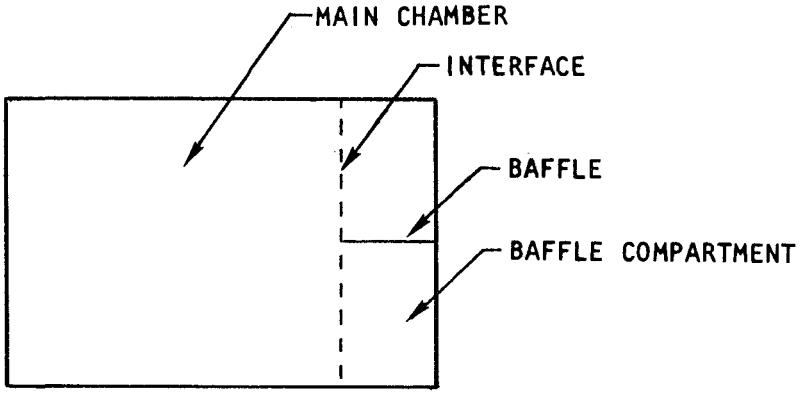

In an effort to satisfy the pressure condition as well as possible, three different kinds of approximate functions were used. In the first of these, the pressure distribution on the main-chamber side of the interface was assumed to be of the form $\cos \bar{m}\pi y/W$. Secondly, a similar distribution was assumed for the compartment side. Neither of these resulted in a good pressure match; therefore, the iteration scheme was developed to improve the agreement.

MAIN-CHAMBER APPROXIMATION

With the main-chamber approximation (i.e., assumed pressure profile on chamber side) the following characteristic equation was obtained (see Appendix B) for equal length and equally spaced baffles.

$$\frac{\varepsilon_{\bar{m}}/W}{k_{\bar{m}} \tan k_{\bar{m}} L} + \sum_{\mu,q} \frac{\varepsilon_q}{w} \frac{A^2_{\mu q \bar{m}}}{k_q \tan k_q \ell} = 0 \qquad (9)$$

where

$$A_{\mu qm} = \int_{\mu w}^{(\mu+1)w} \cos \frac{q\pi(y_0 - \mu w)}{w} \cos \frac{m\pi y_0}{W} \, dy_0$$

The integral for $A_{\mu qm}$ was evaluated analytically but is written more compactly as shown.

The predicted frequencies obtained from numerical solution of Eq. 9, for the first-transverse mode in the main chamber, are shown in Fig. 1, along with some unpublished acoustic modeling data. These frequency results are not entirely unsatisfactory despite being somewhat low; however, the predicted pressures were entirely unsatisfactory. Calculated pressures on each side of the interface are shown in Fig. 2. Because of the large disparity shown in this figure, the analysis and calculations were carefully checked for errors but none were found. Thus, it was concluded that a better approximation was needed.

BAFFLE-COMPARTMENT APPROXIMATION

The second approximation was developed from an assumed pressure profile of cos $\bar{m}\pi y/W$ on the compartment side of the interface. A somewhat more complicated characteristic equation was obtained (see Appendix B):

$$\sum_m \frac{\varepsilon_m}{W} \frac{\left\{ \sum_{\mu,q} \frac{\varepsilon_q}{w} (k_q \tan k_q \ell) A_{\mu q \bar{m}} A_{\mu q m} \right\}^2}{k_m \tan k_m L} + \qquad (10)$$

$$\sum_{\mu,q} \frac{\varepsilon_q}{w} (k_q \tan k_q \ell) A^2_{\mu q \bar{m}} = 0$$

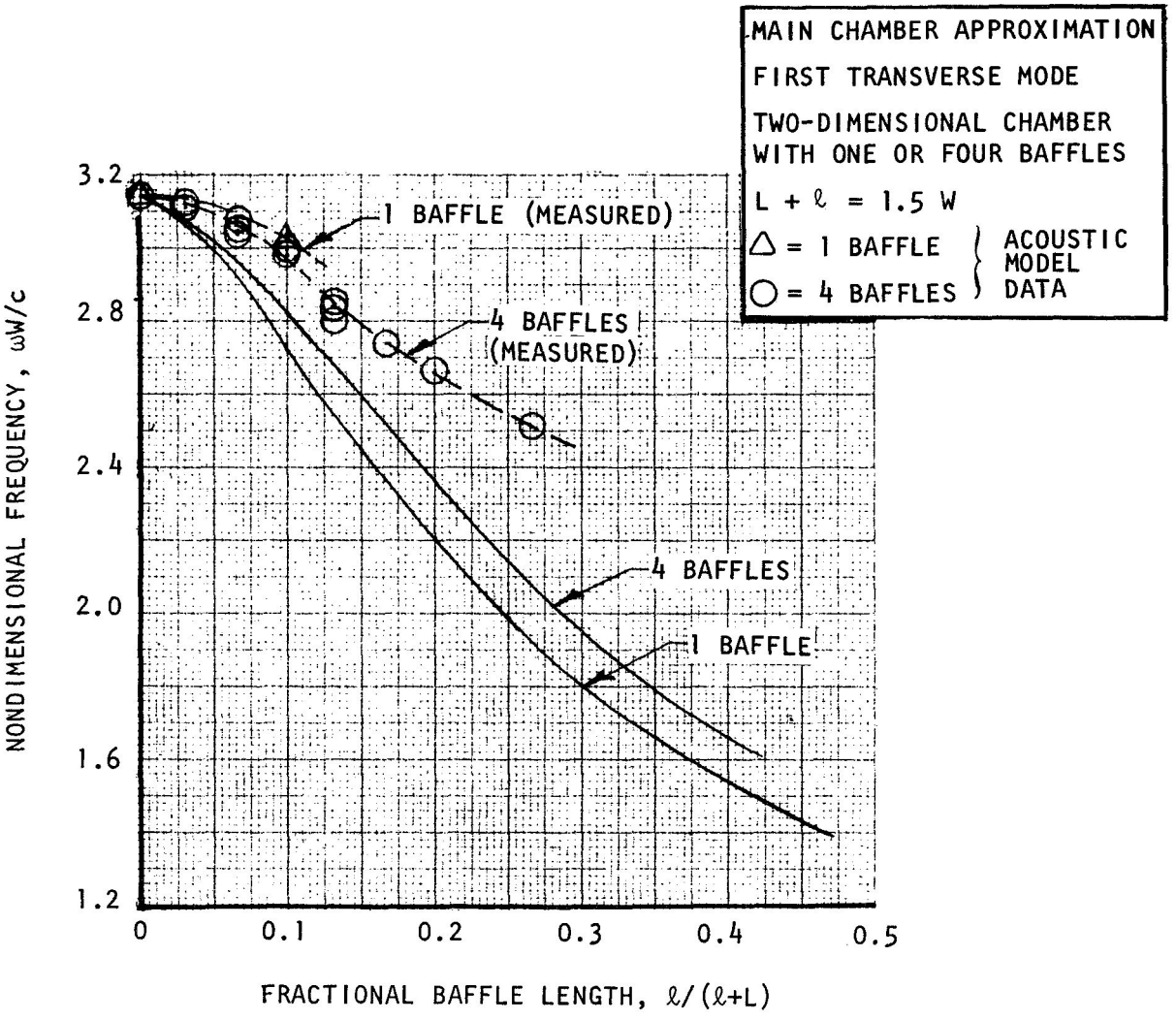

Figure 1. Predicted Frequency Dependence on Baffle Length From the Main Chamber Approximation

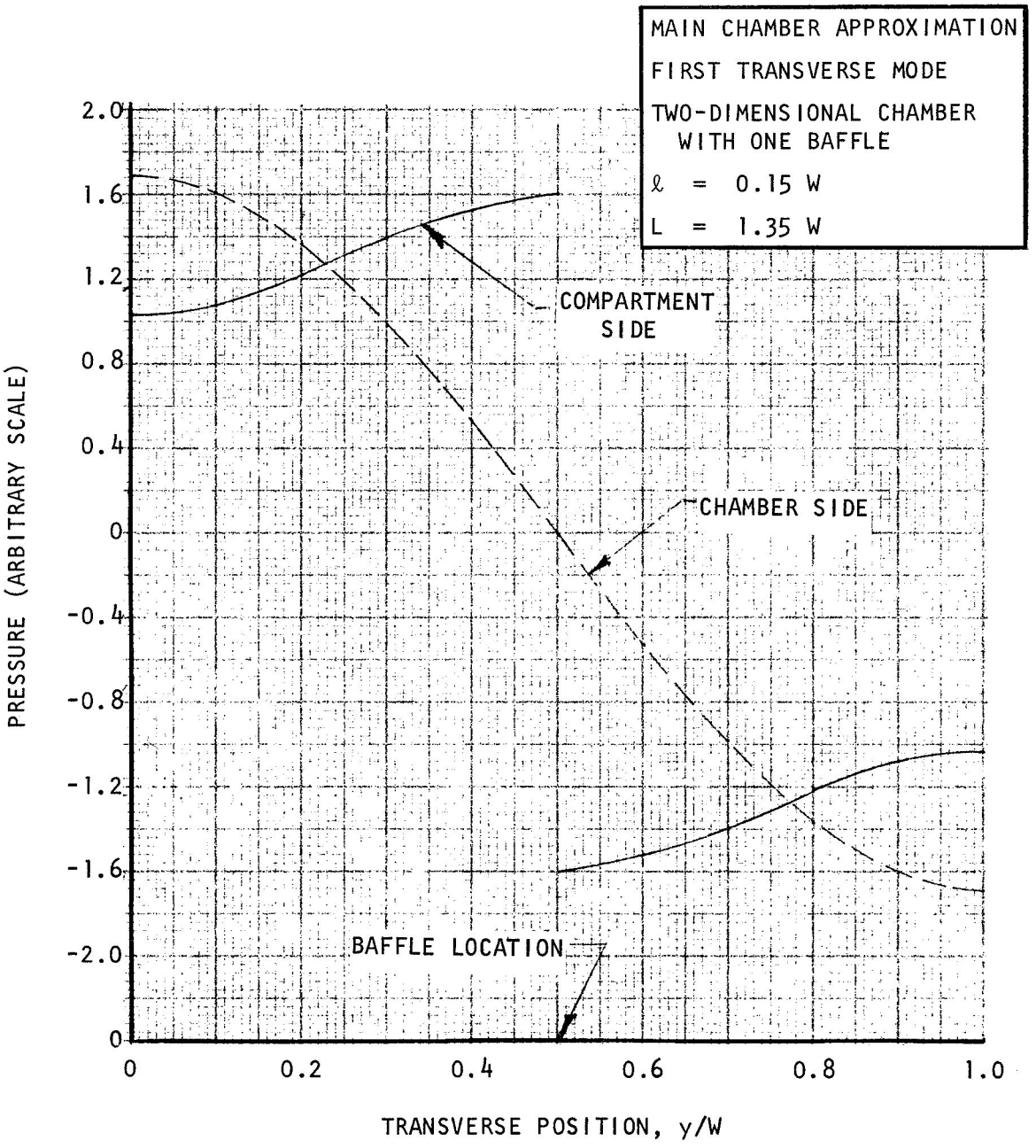

Figure 2. Predicted Pressure Profiles on Each Side of the Main Chamber-Compartment Interface From the Main-Chamber Approximation

The pressure distribution on the compartment side of the interface for the μ^{th} compartment was given by

$$p_{b\mu}(L,y) = \sum_q \frac{\varepsilon_q}{w} \cos \frac{q\pi(y - \mu w)}{w} A_{\mu q \bar{m}} \qquad (11)$$

which is merely a Fourier series representation of cos $\bar{m}\pi y/W$. When numerical solution of Eq. 10 was attempted, no solutions were found to exist unless only the first term in q was retained, in which case all coefficients in the Fourier series (Eq. 11) are zero except the first. Thus, the pressure match at the interface was poor in this case as well; exemplary results are shown in Fig. 3. However, the frequency results improved.

The iterative calculations were made with this compartment approximation as a starting condition, i.e., a zeroth iteration.

ITERATIVE APPROXIMATION

The characteristic equation obtained in this case (Appendix B) is the same as that shown in Eq. 10 except the coefficients $A_{\mu q \bar{m}}$ are replaced by an $a_{\mu q}^{(n+1)}$, where

$$a_{\mu q}^{(n+1)} = -\sum_m \frac{\varepsilon_m}{W} \frac{\left\{\sum_{\mu,q} \frac{\varepsilon_q}{w} (k_q \tan k_q \ell) A_{\mu q m} a_{\mu q}^{(n)}\right\}}{k_m \tan k_m L} A_{\mu q m} \qquad (12)$$

and

$$a_{\mu q}^{(0)} = A_{\mu q \bar{m}}$$

The frequencies obtained by numerical solution of this characteristic equation for the first-transverse, main-chamber mode are shown in Fig. 4, along with the acoustic modeling data. The curve denoted by "zero iterations" is the result from the compartment approximation just described. Agreement

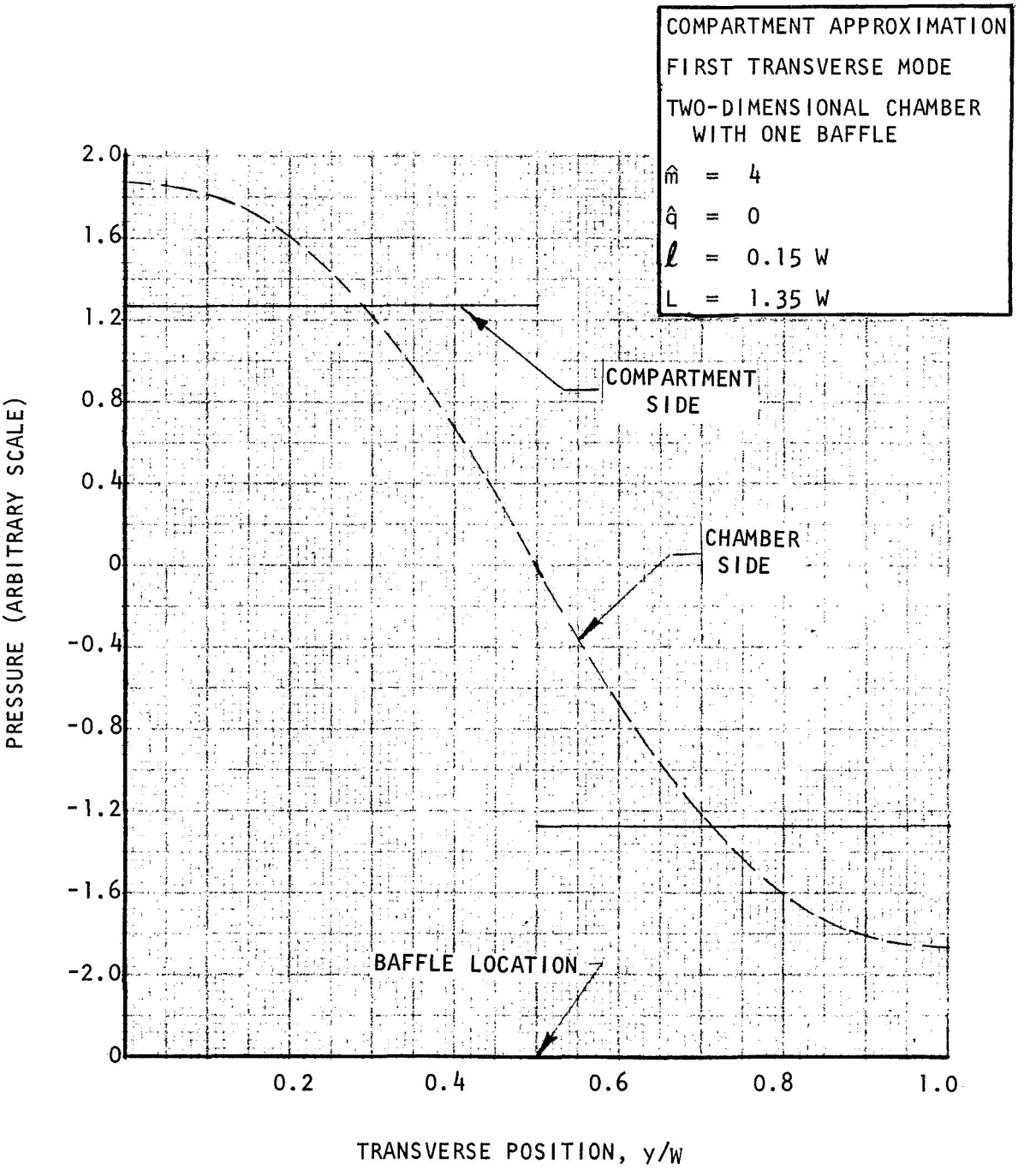

Figure 3. Predicted Pressure Profiles on Each Side of the Interface From the Compartment Approximation

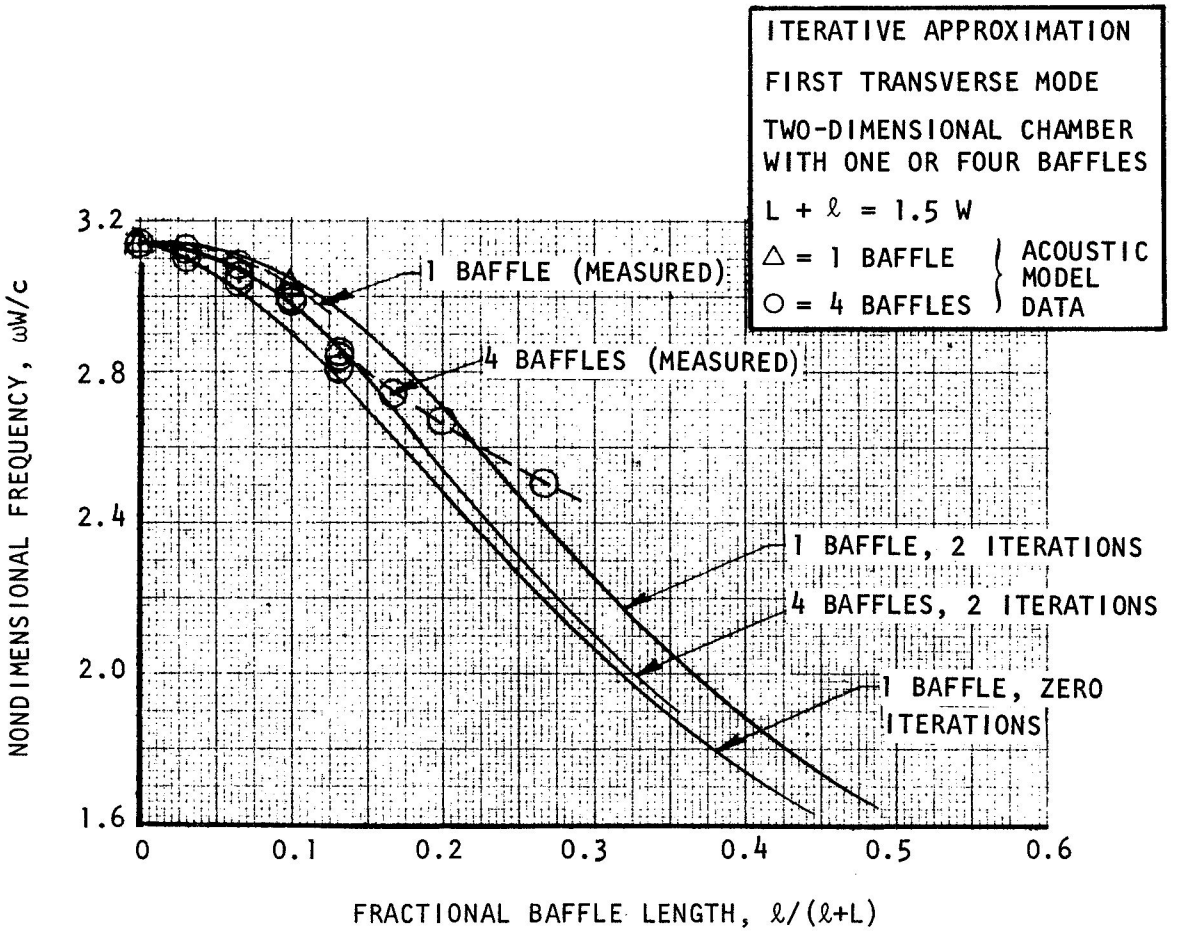

Figure 4. Predicted Frequency Dependence on Baffle Length From the Iterative Approximation

between predicted and measured frequencies is quite good. The data show a somewhat higher trend at the longer baffle lengths, but this is believed to be due to intercompartmental leakage in the acoustic model.

The modeling data were obtained from a two-dimensional rectangular model (20 x 30 centimeters) with one or four baffles of (approximately) equal length and spacing mounted in one end. The largest share of these data (those obtained with four baffles) were obtained with relatively loose-fitting baffles. This lack of snug fit is likely to have caused some error in experimental results, especially with long baffles, because of intercompartmental leakage. A frequency depression similar to that shown by these data has been observed repeated in engine tests and in other modeling tests (for example see Ref. 5).

The characteristic equation as written in Eq. 10 and previously in Eq. 4, represents an overall energy balance. However, it appears more appropriate to consider an individual balance for each compartment. If this is done, the characteristic equation is similar to Eq. 10 except one summation over μ is removed from each term. Fortunately, calculations made in this manner yielded the same frequencies as the overall equation. Thus, it was not necessary to worry about selecting the best "average" frequency.

A satisfactory pressure match across the interface was obtained from the iterated calculation. Typical results are shown in Fig. 5 and 6 for chambers containing one and four baffles, respectively. Note that the error appears to diminish as the number of baffles contained in the chamber is increased. Hopefully, with a large enough number of terms in each series, and with sufficient iterations, exact agreement in the pressures can be obtained.

A limited attempt to show a trend toward such convergence was somewhat discouraging, however. The average pressure difference (rms) between the two sides of the interface was calculated for one baffle configuration,

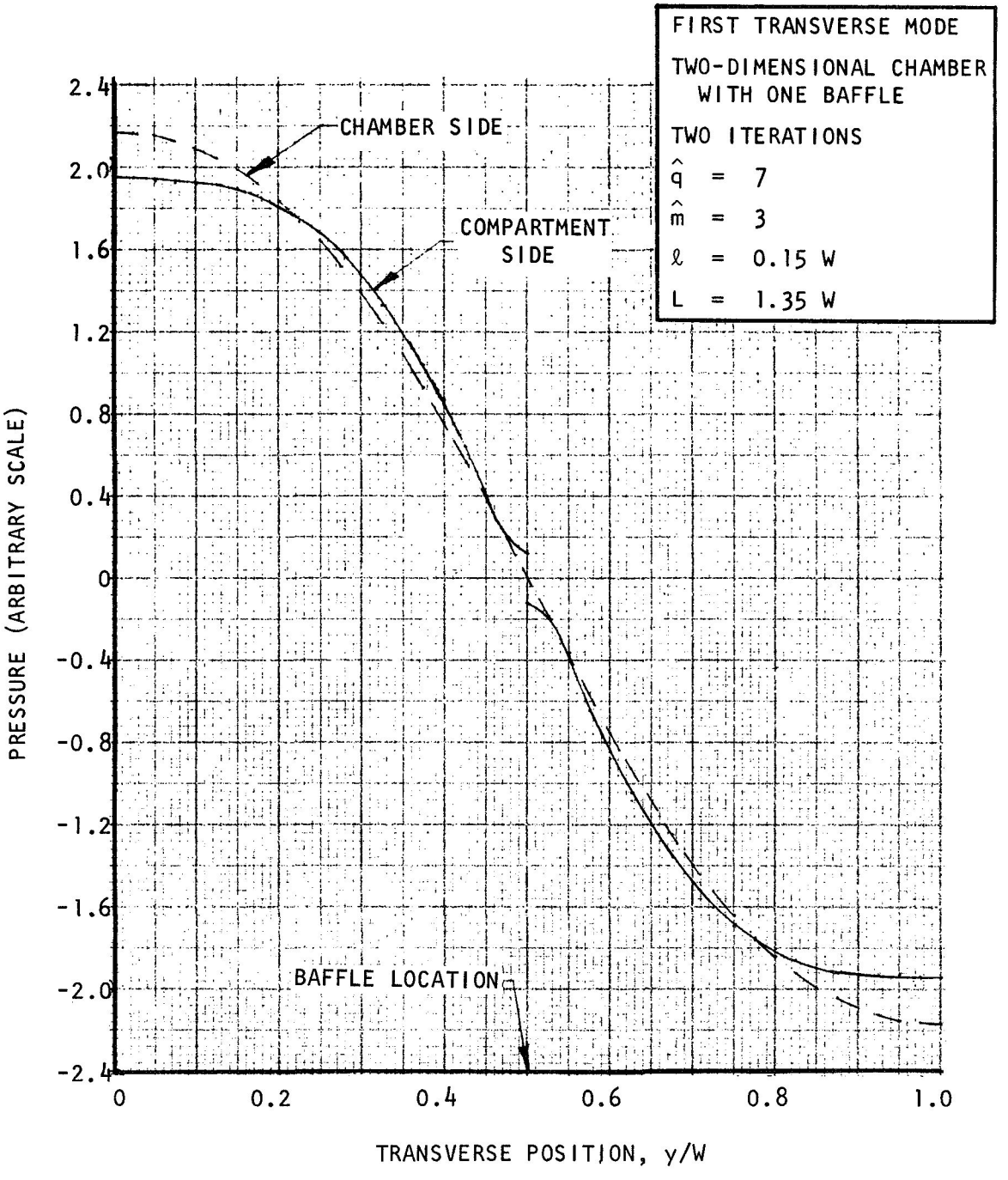

Figure 5. Predicted Pressure Profiles for a Single Baffle From the Iterative Approximation

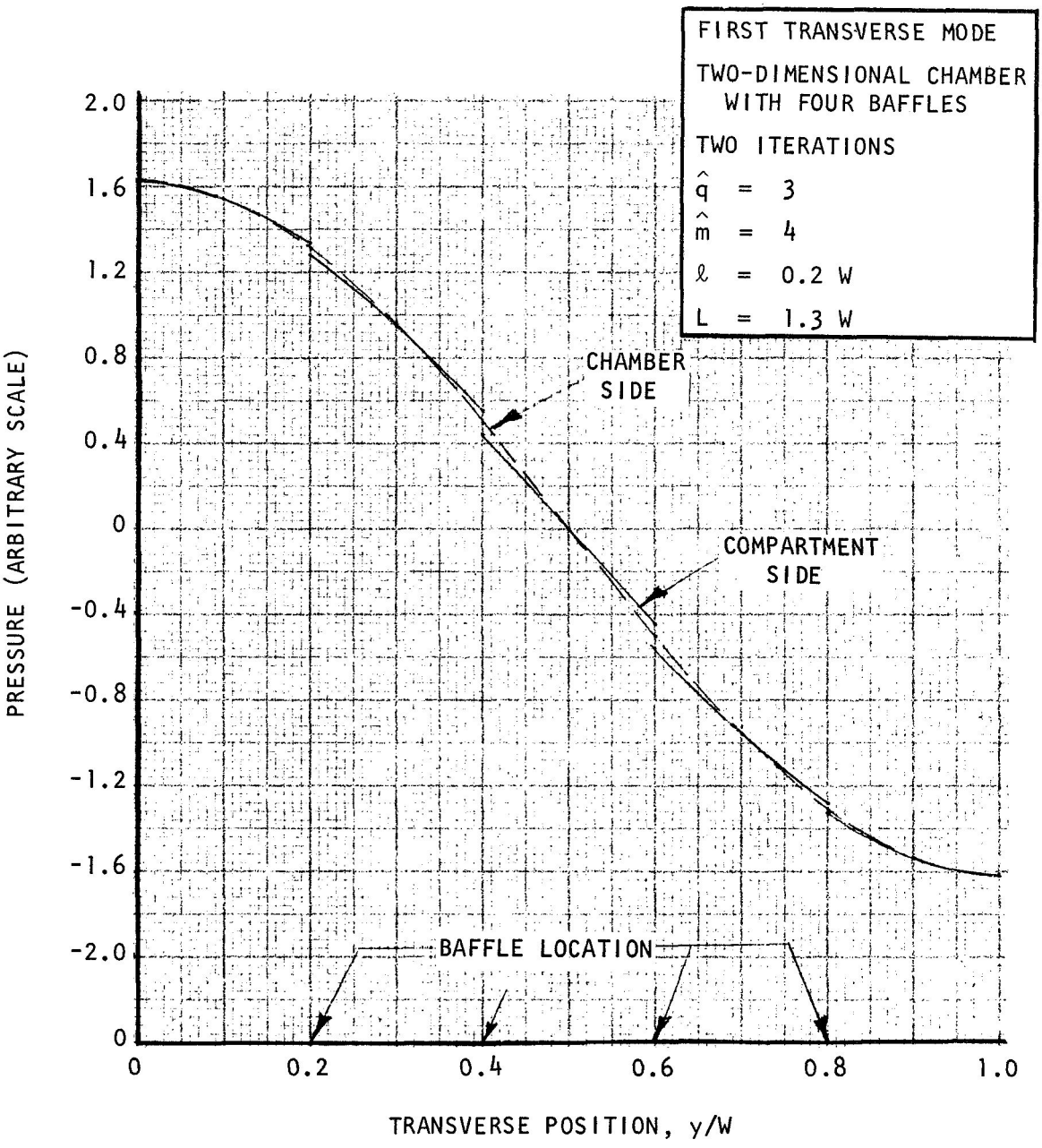

Figure 6. Predicted Pressure Profiles for Four Baffles From the Iterative Approximation

while the number of terms in m and q and the number of iterations were individually varied from a base combination. The configuration was a single 3-centimeter-long baffle in one end of a 20- by 30-centimeter chamber. The results (Fig. 7, 8 and 9) show that the errors are reasonably low, but they exhibit a disturbing trend toward increased error with increased q and, to some extent, with the number of iterations. However, these effects have not been properly investigated; convergence may indeed occur with a simultaneous increase in each of these terms. Further, the results may be affected by the small number of terms retained, which was necessary because of the small capacity of the time-sharing computer used to solve the equation.

Based on the iterative method, pressure profiles were calculated at several longitudinal positions in the chamber. The results are shown in Fig. 10 along with acoustic modeling data. The calculated profiles are symmetrical, whereas the measured profiles are not, probably because the baffle was not exactly centered and the model was driven from one side ($x = 1.5$ cm and $y = 0$). Nevertheless, the agreement is regarded as good.

Little attention was given to the possibility of calculating baffle compartment modes. However, such a mode was indicated in some of the calculations. The results are not presented here because the pressure match at the interface was poor.

TWO-DIMENSIONAL CHAMBERS WITH GAIN/LOSS BOUNDARY CONDITIONS

The effects of pressure-coupled gains and losses were simulated to a degree by adding nonzero acoustic admittance values at both ends of the chamber. A loss-type condition was imposed at the nozzle end and a gain-type condition at the injector end. These effects were added so that the influence of baffles on (pressure-coupled) stability could be investigated. Because no steady flow was included in the calculation, effective or virtual boundary conditions were used to compensate for the omission. However, this distinction between actual and virtual boundary conditions only affects the choice of numerical values to be examined and, hence, is of little importance.

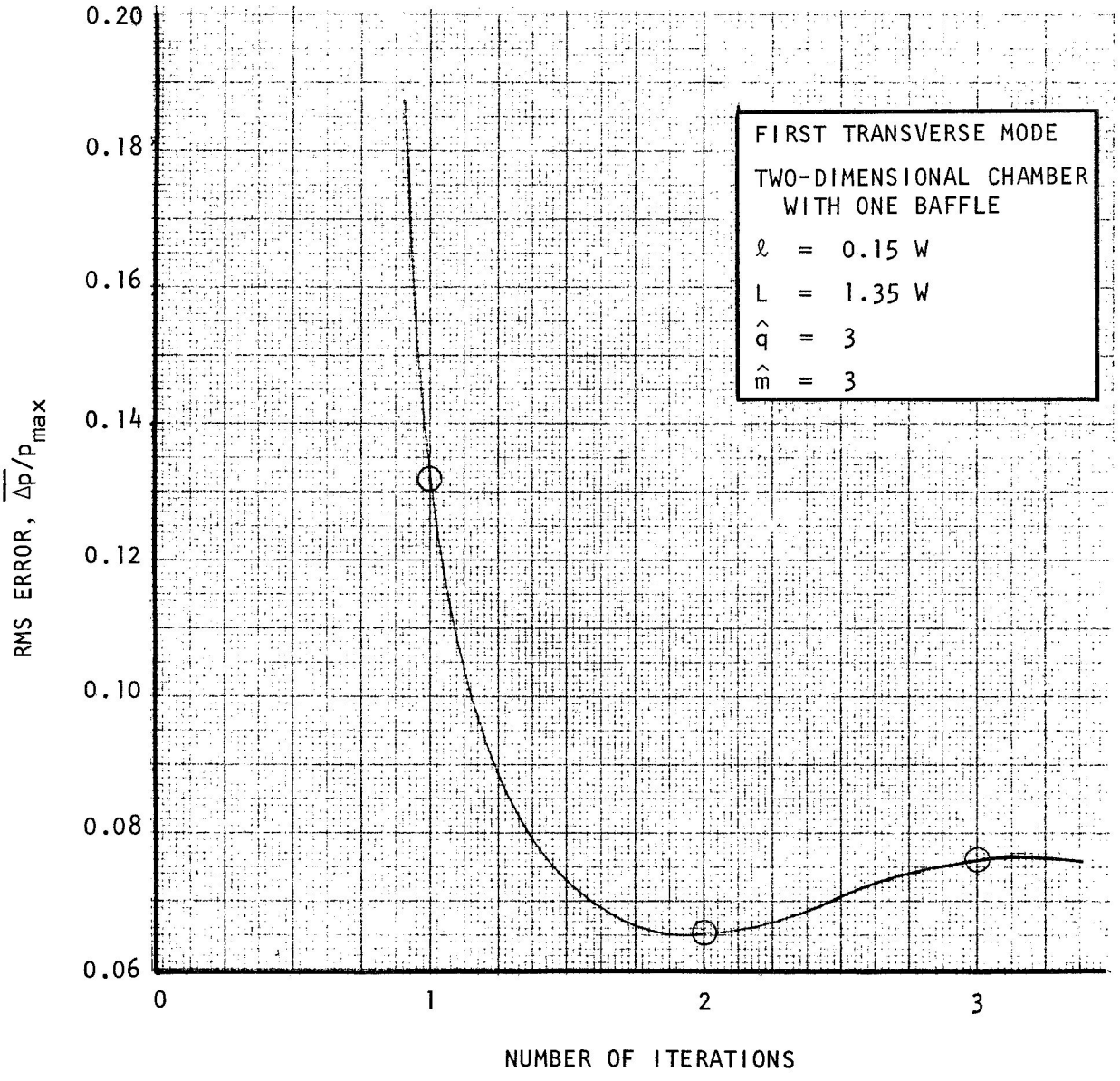

Figure 7. Dependence of Error on Number of Iterations

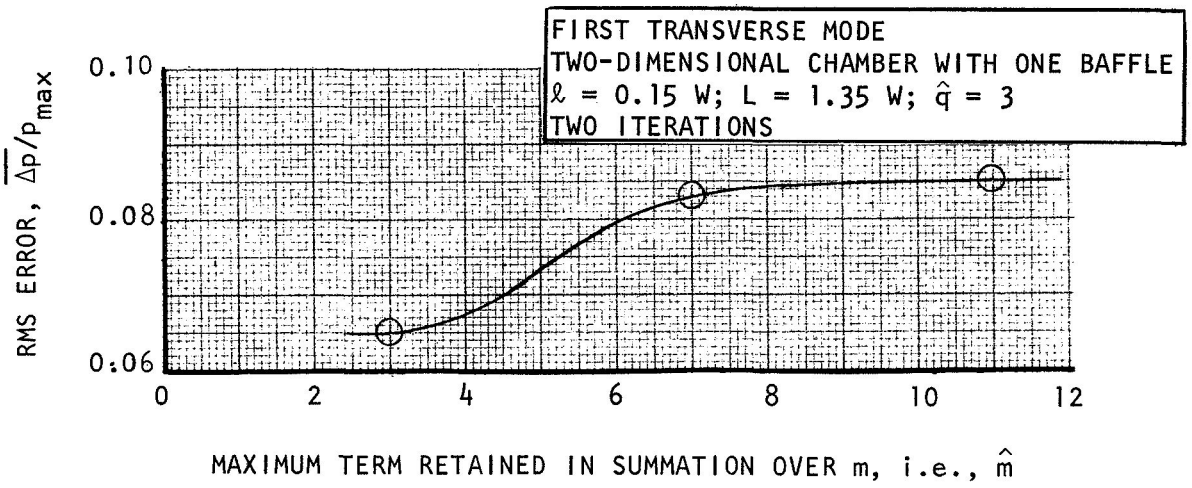

Figure 8. Dependence of Error on Number of Terms in m Retained

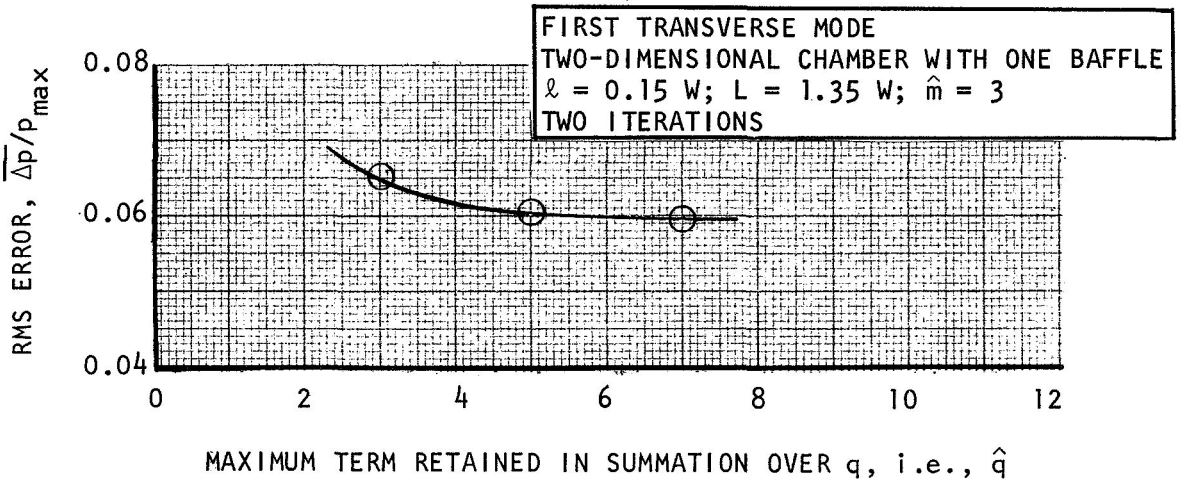

Figure 9. Dependence of Error on Number of Terms in q Retained

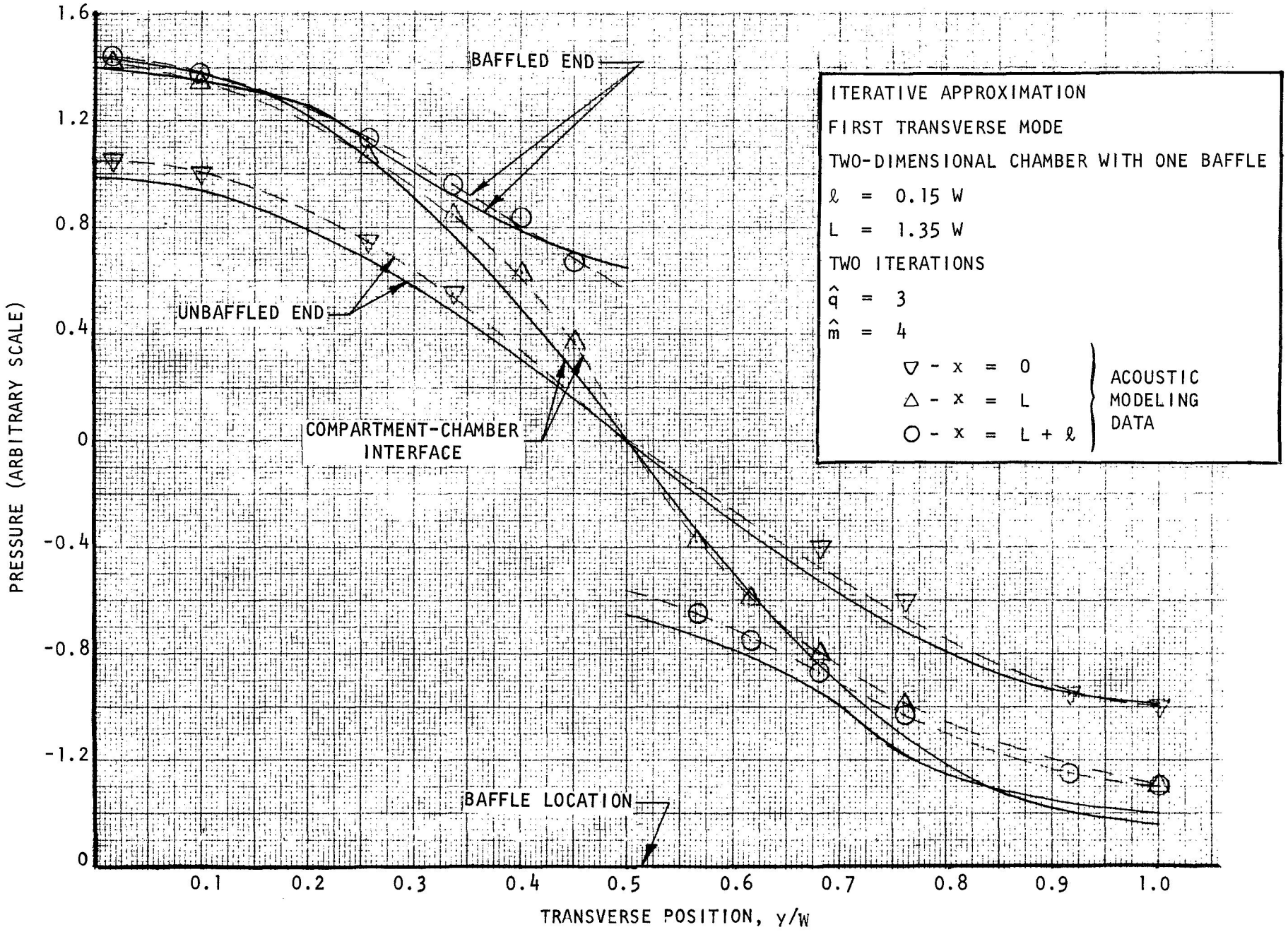

Figure 10. Comparison Between Measured and Predicted Pressure Distributions for Baffled Chamber

The boundary condition was written in terms of a specific acoustic admittance:

$$y = \rho c \frac{\vec{N}\cdot\vec{u}}{p} \tag{13}$$

To partially compensate for steady through flow at the boundaries, this admittance may be replaced by (Ref. 6 and 7)

$$\rho c \frac{\vec{N}\cdot\vec{u}}{p} = \gamma M \left\{\frac{\mu}{\varepsilon}\right\} \tag{14}$$

where M is the steady-flow Mach number through the boundary and μ/ε is the response function (fractional perturbation in mass flux divided by the fractional perturbation in pressure). Equation 14 was used only to estimate numerical values for the acoustic admittances.

The iterative form of the characteristic equation may be rewritten to include these boundary conditions (see Appendix B). The result is

$$\sum_m \frac{\varepsilon_m}{W} \frac{\left\{\sum_{\mu,q} \frac{\varepsilon_q}{w} k_q \tan(k_q \ell + \psi_q)\, a_{\mu q}^{(n+1)}\, A_{\mu q m}\right\}^2}{k_m \tan(k_m L + \psi_m)} +$$

$$\sum_{\mu,y} \frac{\varepsilon_q}{w} \left\{a_{\mu q}^{(n+1)}\right\}^2 k_q \tan(k_q \ell + \psi_q) = 0 \tag{15}$$

where

$$\tan \psi_m = -jky_N / k_m$$

$$\tan \psi_q = -jky_I / k_q$$

and y_N and y_I are the specific admittance values at the nozzle and injector ends, respectively.

The effects of baffles on the stability of this chamber were investigated by comparing the stability requirements with and without a baffle. For a fixed nozzle loss, the injector-end admittance necessary for neutral stability was calculated, thus defining a stability limit curve. This was done by solving Eq. 15, with a numerical root-finding technique, for the y_I that corresponded to particular, real eigenvalues and a constant nozzle admittance.

A stability limit curve was also calculated for the unbaffled case from

$$-j \frac{k_m}{k} \tan(k_m L + \psi_m) = y_I \tag{16}$$

The nozzle admittance was estimated from that for a zero-length nozzle with an entrance steady-flow Mach number of 0.266 and $\gamma = 1.25$. The response function for a zero-length nozzle is $(\gamma + 1)/2\gamma$; thus, a value of $y_N = 0.3$ was chosen.

Stability limit curves for the unbaffled case and for a single baffle are shown in Fig. 11. As defined, the admittance has a driving effect if the real part of the admittance is negative. Therefore, these calculations indicate the engine is less stable with a baffle than without.

This result is not very surprising in view of the observed effect of baffles on the pressure distribution within the chamber; the baffles increase the amplitude at the injector end relative to the nozzle end. According to Cantrell (Ref. 6), neutral stability is obtained when

$$\int_S p^2 \, \mathrm{Re}\{y\} \, dS = 0 \tag{17}$$

If the amplitude at the injector end is increased, the real part of the admittance at that end must be reduced to balance the same nozzle loss.

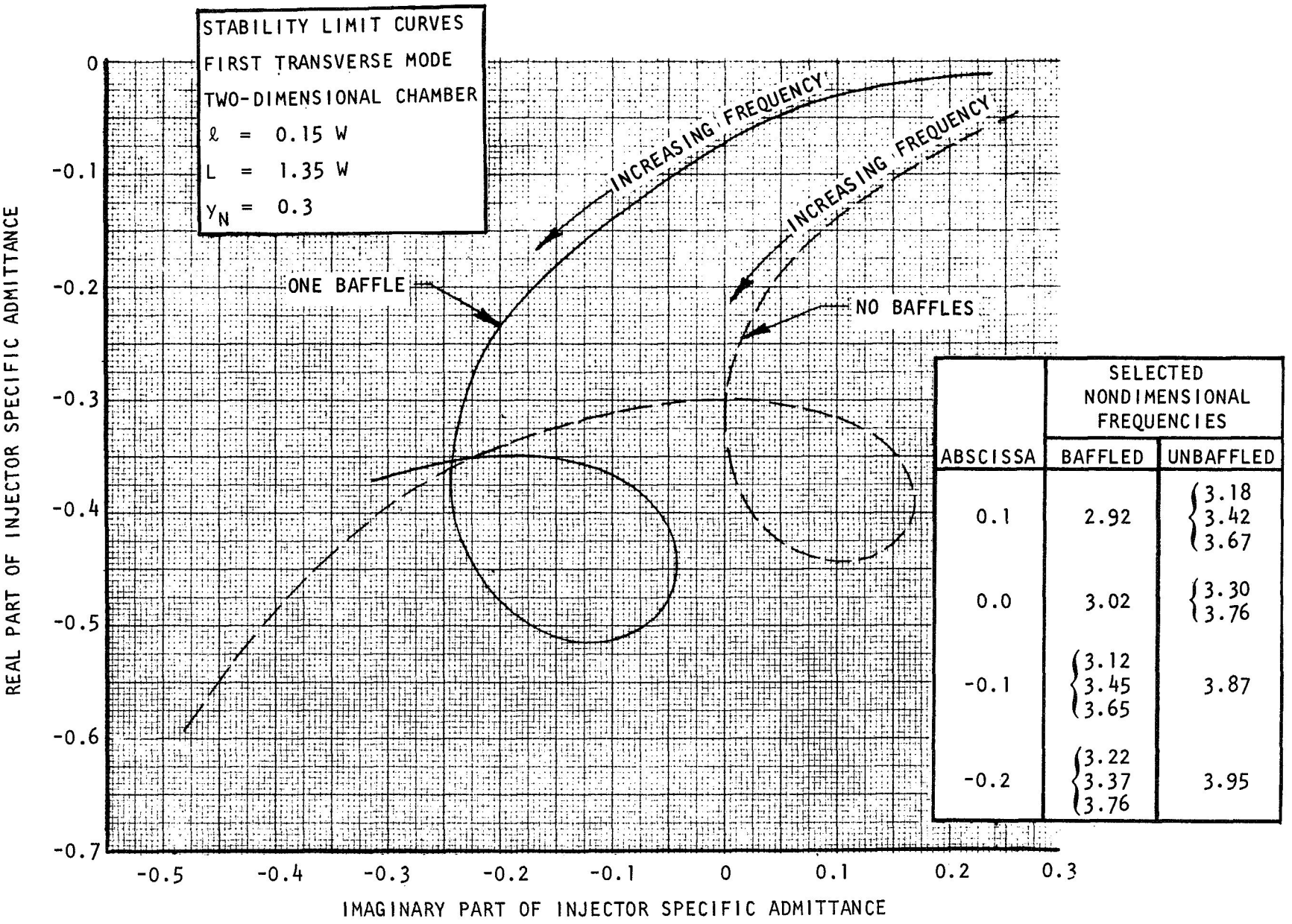

ABSCISSA	SELECTED NONDIMENSIONAL FREQUENCIES	
	BAFFLED	UNBAFFLED
0.1	2.92	3.18 3.42 3.67
0.0	3.02	3.30 3.76
-0.1	3.12 3.45 3.65	3.87
-0.2	3.22 3.37 3.76	3.95

Figure 11. Predicted Effect of One Baffle on Stability Limit

This implies that baffles improve the stability of an engine in some other manner than reducing pressure coupling, at least to the extent that pressure coupling is approximated by an acoustic admittance.

CONCLUSIONS

Results from this study indicate that a largely satisfactory mathematical technique has been developed for calculating the wave motion in baffled chambers. This technique has been applied to several simple cases with good success, but additional work is needed to develop a thorough understanding of the oscillatory behavior of baffled chambers. The ability to obtain an essentially continuous pressure profile along the baffle tips has been demonstrated with this technique. Requirements for continuity of velocity and energy flux at the interface between the baffle compartments and main chamber are automatically satisfied.

The effects of a single baffle on the stability of a chamber with nonrigid walls (gain/loss-type boundary conditions) has been successfully analyzed for one particular geometry. Thus, the ability to generalize the method for nonzero boundary conditions has also been demonstrated. Convergence of the iterational scheme has not been completely demonstrated. However, very good numerical results were obtained and it is likely that adequate convergence can also be obtained. Convergence appears even less restrictive when the chamber contains more than one baffle.

REFERENCES

1. R-7868, by C. L. Oberg and L. P. Combs, Design Criteria Monograph: Liquid Propellant Rocket Engine Combustion Stabilization Devices, Rocketdyne, a Division of North American Rockwell Corporation, Canoga Park, California, May 1969 (not yet approved for distribution).

2. McBride, J. M.: "Blade Arrangement and Blade Design," ICRPG Reference Book on Liquid Propellant Rocket Combustion Instability, Sections 8.2.2 and 8.2.3, 1969 (to be published).

3. Morse, P. M. and H. Feshbach: Methods of Theoretical Physics, McGraw-Hill Book Co., Inc., New York, 1953.

4. Morse, P. M. and K. U. Ingard: Theoretical Acoustics, McGraw-Hill Book Co., Inc., New York, 1968.

5. SSD-TR-66-2, Gemini Stability Improvement Program (GEMSIP), Final Report; Volume 5: Development Tools, Aerojet-General Corp., August 1965.

6. Cantrell, R. H. and R. W. Hart: Interaction Between Sound and Flow in Acoustic Cavities: Mass, Momentum, and Flow Considerations, Jour. Acoust. Soc. Am., Vol. 36, 1964, pp. 697-706.

7. McClure, F. T., R. W. Hart, and R. H. Cantrell: Interaction Between Sound and Flow--Stability of T-Burners, AIAA Jour., Vol. 1, No. 3, March 1963, pp. 586-590.

APPENDIX A

SECULAR EQUATION TECHNIQUE

Morse* suggests approximate solution of integral equations, such as those encountered herein, by assuming an eigenfunction expansion for the dependent variable. A secular determinant is thereby obtained. This approach is more appealing in some respects than the variation-iteration technique described previously because no initial estimate of the solution is required. For this reason, considerable emphasis was placed on this technique during the program. However, satisfactory numerical results were never obtained. The reason for this failure is not known. The method is believed applicable; therefore, the failure may be due to a mathematical or programming error, although both the analysis and the computer program have been checked thoroughly.

Because the secular equation method is still believed applicable, it will be briefly outlined here. Both the Green's functions and the normal gradient (ξ) can be expanded in terms of a convenient set of eigenfunctions; the Green's functions can be written explicitly, but the coefficients in the expansion for ξ are left unspecified. The Green's functions appear as

$$G(\vec{r}|\vec{r}_0) = \sum_n \frac{\phi_n(\vec{r})\ \phi_n(\vec{r}_0)}{V\Lambda_n(\eta_n^2 - k^2)} \tag{A-1}$$

and ξ as

$$\xi(\vec{r}_0) = \sum_m c_m\ \phi_m(\vec{r}_0) \tag{A-2}$$

*Morse, P. M., and K. U. Ingard: Theoretical Acoustics, McGraw-Hill Book Co., Inc., New York, 1968.
Morse, P. M., and H. Feshbach: Methods of Theoretical Physics, McGraw-Hill Book Co., Inc., New York, 1953.

Insertion of Eq. A-2 into the set of integral equations, Eq. 4 , and employing the orthogonality properties of the eigenfunctions, leads to a set of linear algebraic equations in c_m, each equation being equal to zero. Therefore, the determinant of the coefficients of the c_m array must equal zero to give a nontrivial solution. This determinant is a secular determinant; it represents a characteristic equation that specifies the eigenvalues (frequencies) of the combustion chamber.

In principle, the secular determinant is of infinite order, but the indications are that it can be truncated at some reasonable size. Once the eigenvalues are determined, the array of equations in c_m can be solved for each of the coefficients, each c_m, in terms of one of them. The function $\xi(\vec{r}_0)$ is thereby specified and the pressure distribution throughout the combustion chamber may be calculated.

As noted above, the secular-equation formulation was developed and programmed for numerical solution. Initial results were promising, but eventually it was found that unacceptable frequency and pressure results were being obtained. Specifically, a pressure discontinuity was predicted about midway between baffle tips. The reason for this was not found.

APPENDIX B

DEVELOPMENT OF EQUATIONS

In this appendix the mathematical details concerning the variational solution of the wave equation (actually, the Helmholtz equation) for closed, two-dimensional, baffled chambers are summarized. The initial section is concerned with development of the variational form of the characteristic equation, while the second section deals with the development of the approximate velocity distributions necessary for the main-chamber and baffle-compartment approximations. The iteration scheme is also developed therefrom, and finally, the equations for the nonzero admittance case are summarized.

VARIATIONAL FORMULATION

The variational formulation used during this program is patterned closely after that described by Morse and Ingard*. Employing the variational function developed by them, with a slight generalization for multiple cavities, a characteristic equation was obtained.

$$\int_{S_t} \xi \int_{S_t} G_a(\vec{r}|\vec{r}_0)\ \xi\ dS_0\ dS + \int_{S_t} \xi \int_{S_\mu} G_{b\mu}(\vec{r}|\vec{r}_0)\ \xi\ dS_0\ dS = 0 \quad \text{(B-1)}$$

where ξ is proportional to the normal component of velocity at the interface between the main chamber and the compartments. This equation was obtained from the variational method for an approximate normal velocity of the form $u = A\xi$, the value of the amplitude (A) being optimized by the method.

Equation B-1 may be rewritten as

$$\int \xi (p_a - p_{b\mu})\ dS = 0 \quad \text{(B-2)}$$

*Morse, P. M., and K. U. Ingard: Theoretical Acoustics, McGraw-Hill Book Co., Inc., New York, 1968, p 680.

because, except for an arbitrary amplitude coefficient,

$$p_a(\vec{r}) = -j\rho\omega \int_{S_t} G_a(\vec{r}|\vec{r}_0^S)\ \xi(\vec{r}_0^S)\ dS_0 \tag{B-3}$$

$$p_{b\mu}(\vec{r}) = j\rho\omega \int_{S\mu} G_{b\mu}(\vec{r}|\vec{r}_0^S)\ \xi(\vec{r}_0^S)\ dS_0 \tag{B-4}$$

Equation B-2 implies that the best estimates, in the variational sense, of the eigenvalues (frequencies) of the baffled chamber are obtained by requiring continuity of the energy flux at the interface. Thus, requirements for continuity of energy flux and velocity at the interface are automatically satisfied. However, calculated pressures on each side of the interface will not be equal unless the exact normal velocity distribution is used.

Clearly, the next task is to develop a means for finding suitable estimates of the normal velocity distribution. Rather than attempting to choose a velocity distribution directly, however, approximate pressure distributions were selected and the corresponding velocity distributions were calculated.

MAIN-CHAMBER APPROXIMATION

This approximation was obtained by assuming a pressure profile on the main chamber side of the form

$$p_a(L,y) = \cos \frac{\bar{m}\pi y}{W} \tag{B-5}$$

However,

$$p_a(L,y) = \int G_a(\vec{r}^S|\vec{r}_0^S)\ \frac{\partial p_a}{\partial x_0}\ dy_0 \tag{B-6}$$

and

$$G_a(\vec{r}|\vec{r}_0) = -\sum \frac{\varepsilon_m}{W} \frac{\cos \frac{m\pi y}{W} \cos \frac{m\pi y_0}{W}}{k_m \sin k_m L} F_m(x)$$

where

$$F_m(x) = \begin{cases} \cos k_m(x_0 - L) \cos k_m x & x < x_0 \\ \cos k_m x_0 \cos k_m(x - L) & x > x_0 \end{cases} \tag{B-7}$$

Therefore,

$$\frac{\int \frac{\partial p_a}{\partial x_0} \cos \frac{m\pi y_0}{W} dy_0}{-k_m \tan k_m L} = \begin{cases} W/\varepsilon_{\bar{m}} & m = \bar{m} \\ 0 & m \neq \bar{m} \end{cases} \tag{B-8}$$

Further, from the integral expression for p_a,

$$\frac{\partial p_a(L,y)}{\partial x} = \sum \frac{\varepsilon_m}{W} \cos \frac{m\pi y}{W} \int \frac{\partial p_a}{\partial x_0} \cos \frac{m\pi y}{W} dy_0 \tag{B-9}$$

Consequently, from Eq. B-8 and B-9,

$$\frac{\partial p_a(L,y)}{\partial x} = \xi = -k_{\bar{m}} \tan k_{\bar{m}} L \cos \frac{\bar{m}\pi y}{W} \tag{B-10}$$

Introducing this expression into the characteristic equation (Eq. B-1) leads to

$$\frac{\varepsilon_{\bar{m}}/W}{k_{\bar{m}} \tan k_{\bar{m}} L} + \sum_{\mu,q} \frac{\varepsilon_q}{w} \frac{A^2_{\mu q \bar{m}}}{k_q \tan k_q \ell} = 0 \tag{B-11}$$

where

$$A_{\mu q \bar{m}} = \int_{\mu w}^{(\mu+1)w} \cos \frac{\bar{m}\pi y_0}{W} \cos \frac{q\pi(y_0 - \mu w)}{w} \, dy_0$$

COMPARTMENT APPROXIMATION

The compartment approximation was obtained in a similar manner by assuming a compartment-side pressure profile of

$$p_{b\mu}(L,y) = \cos \frac{\bar{m}\pi y}{W} \tag{B-12}$$

for

$$\mu w < y < (\mu + 1)\, w$$

The Green's function for the μ^{th} compartment may be written as

$$G_{b\mu}(\vec{r}|\vec{r}_0) = -\sum_q \frac{\varepsilon_q}{w} \frac{\cos \frac{q\pi(y - w)}{w} \cos \frac{q\pi(y_0 - w)}{w}}{k_q \sin k_q \ell} F_q(x) \tag{B-13}$$

where

$$F_q(x) = \begin{cases} \cos k_q(x_0 - L_t) \cos k_q(x - L) & x < x_0 \\ \cos k_q(x_0 - L) \cos k_q(x - L_t) & x > x_0 \end{cases}$$

$$L_t = L + \ell$$

For this approximation

$$\xi_\mu = \frac{\partial p_{b\mu}}{\partial x} = \sum_q \frac{\varepsilon_q}{w} (k_q \tan k_q \ell) A_{\mu q \bar{m}} \cos \frac{q\pi(y - \mu w)}{w} \tag{B-14}$$

Insertion of this approximation into the characteristic equation (Eq. B-1) leads to Eq. 10. The corresponding pressure expressions were obtained from Eq. B-3 and B-4.

ITERATION SCHEME

Neither of the last two approximations was considered adequate. Therefore, an iteration scheme was developed to improve an initial estimate. A pressure distribution was assumed of the form

$$p_{b\mu}(L,y) = \sum_q \frac{\varepsilon_q}{w} a_{\mu q}^{(n)} \cos \frac{q\pi(y - \mu w)}{w} \qquad \text{(B-15)}$$

for the interval $\mu w < y < (\mu+1)w$.

The corresponding pressure gradient is

$$\frac{\partial p_{b\mu}(L,y)}{\partial x} = \sum_q \frac{\varepsilon_q}{w} a_{\mu q}^{(n)} k_q \tan k_q \ell \cos \frac{q\pi(y - \mu w)}{w} \qquad \text{(B-16)}$$

Further, the corresponding pressure expression for the main chamber side is

$$p_a(L,y) = -\sum \frac{\varepsilon_m}{W} \frac{\cos \frac{m\pi y}{W}}{k_m \tan k_m L} \left\{ \sum_{\mu,q} \frac{\varepsilon_q}{w} a_{\mu q}^{(n)} (k_q \tan k_q \ell) A_{\mu q m} \right\} \qquad \text{(B-17)}$$

Now, by equating the right side of Eq. B-17 to $p_{b\mu}$, an improved estimate may be obtained. From this, the following expression was obtained:

$$a_{\mu q}^{(n+1)} = -\sum_m \frac{\varepsilon_m}{W} \frac{\left(\sum_{\mu,q} \frac{\varepsilon_q}{w} a_{\mu q}^{(n)} k_q \tan k_q \ell \right)}{k_m \tan k_m L} A_{\mu q m} \qquad \text{(B-18)}$$

The characteristic equation obtained in this case is similar to Eq. 10, the only difference being a replacement of $A_{q\bar{m}}$ in that equation by the $a_{\mu q}^{(n+1)}$ shown above.

NONZERO SURFACE ADMITTANCE

The influence of nonzero acoustic admittance boundary conditions at the closed ends of the chamber may be readily included in the analysis by choosing Green's functions which satisfy the same boundary conditions as those satisfied by the pressure. The appropriate Green's functions are then

$$G_a(\vec{r}|\vec{r}_0) = -\sum_m \frac{\varepsilon_m}{W} \frac{\cos\frac{m\pi y}{W}\cos\frac{m\pi y_0}{W}}{k_m \sin(k_m L + \psi_m)} F_m(x) \qquad \text{(B-19)}$$

where

$$F_m(x) = \begin{cases} \cos k_m(L - x_0)\cos(k_m x + \psi_m) & x < x_0 \\ \cos(k_m x_0 + \psi_m)\cos k_m(L - x) & x > x_0 \end{cases}$$

and

$$\tan\psi_m = -jky_N/k_m$$

$$G_{b\mu}(\vec{r}|\vec{r}_0) = -\sum_q \frac{\varepsilon_q}{w} \frac{\cos\frac{q\pi(y - w)}{w}\cos\frac{q\pi(y_0 - w)}{w}}{k_q \sin(k_q \ell + \psi_q)} F_q(x) \qquad \text{(B-20)}$$

where

$$F_q(x) = \begin{cases} \cos[k_q(L_t - x_0) + \psi_q]\cos k_q(x - L) & x < x_0 \\ \cos k_q(x_0 - L)\cos[k_q(L_t - x) + \psi_q] & x > x_0 \end{cases}$$

and

$$\tan \psi_q = -jky_I/k_q$$

When these Green's functions were employed, expressions for pressure and the characteristic equation were obtained which are very similar to the iterative expressions just described, except that the terms $k_q \ell$ and $k_m L$ are replaced by $k_q \ell + \psi_q$ and $k_m L + \psi_m$, respectively. That is, the characteristic equation is

$$\sum_m \frac{\varepsilon_m}{W} \frac{\left\{ \sum_{\mu,q} \frac{\varepsilon_q}{w} k_q \tan(k_q \ell + \psi_q) \, a_{\mu q}^{(n+1)} \, A_{\mu q m} \right\}^2}{k_m \tan(k_m L + \psi_m)} +$$

$$\sum_{\mu,q} \frac{\varepsilon_q}{w} \left\{ a_{\mu q}^{(n+1)} \right\}^2 k_q \tan(k_q \ell + \psi_q) \qquad \text{(B-21)}$$

APPENDIX C

COMPUTER PROGRAMS

This appendix summarizes the four computer programs used during this study Philosphy and derivation of the working equations were described previously in the main body of this report. This appendix describes the numerical methods used to solve these equations, and includes input, output, and operational information as well. The nomenclature of all four programs is closely related and is presented in the Nomenclature subsection.

The four computer programs used in this study are:

1. SSMCE4--solves the characteristic equation for the rigid boundary case
2. SSBPD2--calculates the pressure on the main chamber side of the interface across the baffle tips
3. SSVEL2--calculates the pressure on the compartment side of the interface across the baffle tips
4. SSMCE8--solves the characteristic equation for the active boundary case

These four programs were run on a timesharing computer system (General Electric 420 computer). All four computer programs are not written efficiently with respect to running time; some statements could be eliminated without inhibiting the calculations. This is especially true for programs SSBPD2, SSVEL2, and SSMCE8. The reason for the inefficiency is that the main portion of each of these was pirated from program SSMCE4.

SSMCE4

Computer program SSMCE4 was written to solve the iterative characteristic equation for the rigid boundary case. The method used to solve this

equation was to calculate the value of the function while incrementally changing"phee"(ϕ) until the value of the function changed signs. The usual practice was to calculate the characteristic equation over a large interval by taking large increments of "phee." After noting the interval in which the value of the function changed signs, that interval was subdivided into smaller increments. The procedure was repeated until an accurate value of PHEE was obtained.

The four subroutines used to calculate repetitive terms are:

1. Subroutine TAN(a,b,c) = $k_i \tan k_i \ell$
2. Subroutine TANH(a,b,c) = $-k_i \tanh k_i \ell$
3. ARG(a,b,c,---x) = $A_{\mu q m}$
4. ARI(a,b,c,---x) = $a_{\mu q}$

The computer program names for the various parameters in the characteristic equation are presented in the Nomenclature subsection of this appendix.

The input information required is:

1. PHEE1 = Starting phee value
2. ICON = Index for transfer
3. NUMB = Number of points (phee values) at which the function will be evaluated
4. STEP = Increment for increasing phee from the initial value
5. MU1 = Index of the baffle compartment being examined
6. NS = Number of iterations on $a_{\mu q}$
7. Q1MAX = Number of q+1 terms taken in the $a_{\mu q}$ iteration
8. MUMAX = Total number of baffle compartments
9. QUMAX = Total number of q+1 terms taken in the evaluation of the characteristic equation

10. MMAX = Total number of m+1 terms taken in the evaluation of the characteristic equation

11. MBAR = Index of the particular acoustic mode to be investigated

12. SMLW = Width of a baffle compartment

13. WDTH = Width of the main chamber

14. SMLEL = Length of the baffles

15. XLNGTH = Total length of the chamber

Output from SSMCE4 includes the phee value and the corresponding value of the characteristic equation.

SSBPD2

This program calculates the pressure across the baffle tips on the main chamber side of the interface, and was written for Eq.B-17. With the phee value fixed for a given set of parameters (solution from SSMCE4), Eq. B-17 is an explicit relationship between pressure and the position coordinate (y). Pressure at the baffle tips was calculated across the width of the chamber.

Input for SSBPD2 is the same as that for SSMCE4. The phee value input for SSBPD2 is the root obtained from SSMCE4 for a given set of parameters. Output from SSBPD2 includes pressure and the corresponding values of y.

SSVEL2

This program was used to calculate the pressure at the baffle tips on the compartment side of the interface. Equation B-15 describes this pressure Again, for a given phee value, the pressure is a function of the position coordinate (y). Thus, for a fixed set of parameters, the pressure can be readily calculated for a given y.

Input to SSVEL2 is the same as that for SSBPD2, with the following additions:

y = Initial starting point of y

Step = The incremental step in y

SMLEL1 = SMLEL (nonfunctional parameter)

Output includes pressures ($p_{b\mu}$) and the corresponding position coordinate (y).

SSMCE8

This program was written to determine the stability limit of a combustion chamber with active boundaries located at both ends. The characteristic equation is in complex notation, and the root of the characteristic equation is complex eigenvalue (the real part is the nondimensional frequency and the imaginary part is the nondimensional damping coefficient). The characteristic equation for the active boundary case is given by Eq. B-21. Thus, for a given set of parameters, nozzle admittance, and injector admittance, the complex root which satisfies the characteristic equation specifies the frequency and the damping coefficient of the system. However, for the stability limit of the system, another route can be taken. Because the damping coefficient is zero, the above equation can be solved for y_I rather than ϕ, with fixed values of y_N and phee (REAL). The acoustic admittance thus obtained defines the maximum amount of acoustic energy (related to the admittance) that can be pumped into the system and still have the system stable. This avenue was taken to evaluate the stability limit.

The root-finding technique used to determine y_N was Newton's method, with a finite-difference approximation for the derivative.

With this approximation, a computer program was generated from SSMCE4 with a few alterations. Convergence was not rapid but was sufficient.

The program was written using complex algebra. The input parameters for SSMCE8 included the input for SSMCE4 and admittance. However, y_N, y_I, and phee are complex numbers in this program. Output includes the y_I's and the corresponding values of the characteristic equations.

NOMENCLATURE

	SSMCE4	SSBPD2	SSVEL2	SSMCE8
ε_m	EPM	EPM	EPM	EPM
m	M	M	M	M
W	WDTH	WDTH	WDTH	WDTH
μ	MU	MU	MU	MU
q	QU	QU	QU	QU
ε_q	EPQ	EPQ	EPQ	EPQ
w	SMLW	SMLW	SMLW	SMLW
k_q tan $k_q \ell$	Subroutine TAN	Subroutine TAN	Subroutine TAN	Subroutine TAN
$a_{\mu q}$	Subroutine ARI	Subroutine ARI	Subroutine ARI	Subroutine ARI
$A_{\mu qm}$	Subroutine ARG	Subroutine ARG	Subroutine ARG	Subroutine ARG
L	XLNGTH	XLNGTH	XLNGTH	XLNGTH
ℓ	SMLEL	SMLEL	SMLEL	SMLEL
ϕ	PHEE1	PHEE1	PHEE1	*PHEE1
$k = \phi/w$	PHEE	PHEE	PHEE	*PHEE
π	PI	PI	PI	PI
p_a		FIRSUM		
y		y-coordinate	y-coordinate	
$p_{b\mu}$			QUSUM	
y_q				*YQ
y_m				*YMA

*Complex numbers

```
SSMCE4    09:07  RØCKET  1(,1969


'KEY
50C    CHARACTERISTIC EQ'N FØR THE BAFFLE PRØBLEM
55 INTEGER QU,QQ,QUMAX,QU2,Q1MAX
56 DIMENSIØN RET9(20,20,1),X1(20,20,1)
57
60 10 PRINT 915
65 915 FØRMAT(1HO,2X,26HINPUT: PHEE,IC0N,NUMB,STEP)
70 INPUT,PHEE1,IC0N,NUMB,STEP
71 PRINT 917
72 917 FØRMAT(1HO,2X,19HINPUT: MU1,NS,Q1MAX)
73 INPUT,MU1,NS,Q1MAX
75 IF(IC0N)20,20,30
76 30 PRINT 916
77 916 FØRMAT(1HO,2X,51HINPUT:MUMAX,QUMAX,MMAX,MBAR,WDTH,
78&SMLW,SMLEL,XLNGTH )
79 INPUT,MUMAX,QUMAX,MMAX,MBAR,WDTH,SMLW,SMLEL,XLNGTH
80 PHEE=PHEE1/WDTH
81 20 PRINT 910
82 N=1
83 PRINT 911
84 PRINT 918,PHEE1,WDTH,SMLW,SMLEL,XLNGTH
85 PRINT 912
86 PRINT 919,MMAX,MUMAX,QUMAX,MBAR
87 PRINT 913
88 FMBAR=3
89 15 DØ 170 MU2=1,MUMAX
90 DØ 171 QU2=1,QUMAX
92 FMBAR=FLØAT(MBAR)
93 PI=3.141592
94 RET9(QU2,MU2,MBAR)=0.
95 171 CØNTINUE
96 170 CØNTINUE
97 DØ 172 MU2=1,MUMAX
98 QU2=1
99 FMU2=FLØAT(MU2-1)
101  FQU2=FLØAT(QU2-1)
102  IF(FMBAR)21,21,22
103 22  IF(FQU2)31,31,32
104 21  IF(FQU2)33,33,34
105 33 RET9(QU2,MU2,MBAR)=SMLW
107 GØ TØ 11
108 34 RET9(QU2,MU2,MBAR)=0.0
109 GØ TØ 11
110 PRINT 911
111 31  XI=FMBAR*PI/WDTH
112 RET9(QU2,MU2,MBAR)=(SIN(XI*(FMU2+1.0)*SMLW)
113&-SIN(XI*FMU2*SMLW))/XI
114 GØ TØ 11
```

```
115 32 JK=FQU2
116 XA=(-1.0)**JK
117 XF=FQU2*PI/SMLW
118 XB=FMBAR*PI*SMLW/WDTH
119 XC=XB*FMU2
120 PRINT 912
121 XD=XB*(FMU2+1.0)
122 XE=FMBAR*PI/WDTH
123 IF(XE-XF)58,59,58
124 59 RET9(QU2,MU2,MBAR)=SMLW*COS(FMU2*FQU2*PI)/2.0
125 GO TO 11
126 58 XG=XE/(XF*XF-XE*XE)
128 RET9(QU2,MU2,MBAR)=XG*(SIN(XC)-XA*SIN(XD))
129 11 CONTINUE
131 173 CONTINUE
132 172 CONTINUE
133 CALL ARI(PHEE,WDTH,SMLEL,SMLW,XLNGTH,RET9,
134&MUMAX,QUMAX,MMAX,MBAR,MU1,NS,Q1MAX,FMUD,FQUD,X1)
135 PI=3.141592
140 FIRSUM=0.0
145 DO 200 M=1,MMAX
150 FM=FLOAT(M-1)
155 AA=FM*PI/WDTH
160 DISCR=PHEE*PHEE-AA*AA
165 IF(DISCR)50,51,52
170 50 ART=SQRT(-DISCR)*XLNGTH
175 IF(ART-4.)850,851,851
180 850 CALL TANHY(DISCR,XLNGTH,RET)
185 GO TO 852
190 851 RET=-SQRT(ABS(DISCR))
195 852 GO TO 300
200 51 PRINT 980
205 GO TO 10
210 52 CALL TAN(DISCR,XLNGTH,RET)
211 300 SMUSUM=0.0
212 DO 220 MU=1,MUMAX
213 FMU=FLOAT(MU-1)
215 QSUM=0.0
216 CSUM=0.0
220 DO 210 QU=1,QUMAX
225 FQU=FLOAT(QU-1)
230 IF(FQU)60,60,62
235 60 EPQU=1.0
240 GO TO 301
245 62 EPQU=2.0
250 301 AB=FQU*PI/SMLW
255 DISCR2=PHEE*PHEE-AB*AB
260 IF(DISCR2)65,66,67
265 65 ARP=SQRT(-DISCR2)*SMLEL
270 IF(ARP-4.)860,861,861
275 860 CALL TANHY(DISCR2,SMLEL,RET2)
```

```
280 GØ TØ 347
285 861 RET2=-SQRT(ABS(DISCR2))
286 GØ TØ 347
290 66 PRINT 980
295 GØ TØ 10
300 67 CALL TAN(DISCR2,SMLEL,RET2)
330 347 FMBAR=FLØAT(MBAR)
331 CALL ARG(FQU,FMU,FM,SMLW,WDTH,RET3)
333 FQR=0.0
336 FMUD=FMU
337 FQUD=FQU
341 QSUM=QSUM+EPQU*RET2*RET3*X1(QU,MU,MBAR)/SMLW
342
344 FMU1=FLØAT(MU1-1)
345 210 CØNTINUE
346 IF(FMU-FMU1)4,5,4
347 5 DSUM=QSUM
355 4 SMUSUM=SMUSUM+QSUM
360 220 CØNTINUE
365 IF(FM)70,70,71
370 70 EPM=1.0
375 GØ TØ 303
380 71 EPM=2.0
385 303 FIRSUM=FIRSUM+SMUSUM*DSUM*EPM/(RET*WDTH)
390 200 CØNTINUE
400 SECSUM=0.0
405 MU=MU1
406 FMU=FLØAT(MU)
410 FMU=FLØAT(MU-1)
415 FISUQU=0.0
420 DØ 240 QU=1,QUMAX
425 FQU=FLØAT(QU-1)
430 IF(FQU)80,80,81
435 80 EPQU=1.0
440 GØ TØ 500
445 81 EPQU=2.0
450 500 AC=FQU*PI/SMLW
455 DISCR3=PHEE*PHEE-AC*AC
460 IF(DISCR3)90,91,92
465 90 ARS=SQRT(-DISCR3)*SMLEL
470 IF(ARS-4.)400,401,401
475 400 CALL TANHY(DISCR3,SMLEL,RET5)
480 GØ TØ 410
485 401 RET5=-SQRT(ABS(DISCR3))
486 GØ TØ410
490 91 PRINT 980
495 GØ TØ 10
500 92 CALL TAN(DISCR3,SMLEL,RET5)
579 410 FQP=0.0
583 FMUD=FMU
584 FQUD=FQU
```

```
600 FISUQU=FISUQU+RET5*X1(QU,MU,MBAR)*X1(QU,MU,MBAR)*
601&EPQU/SMLW
605 240 CONTINUE
615 SECSUM=SECSUM+FISUQU
617 953 FORMAT(F12.6)
626 TOSUM=FIRSUM+SECSUM
627 PHEE1=PHEE*WDTH
630 PRINT 952,N,PHEE1,TOSUM
635 IF(N-NUMB)975,975,976
640 975 N=N+1
645 PHEE=PHEE+STEP
650 GO TO 15
655 976 GO TO 10
660 910 FORMAT(35HINITIAL VALUES FOR THIS CALCULATION//)
665 911 FORMAT(1HO,3X,4HPHEE,4X,4HWDTH,4X,5HSMLW ,3X,5HSMLEL,
666&2X,6HXLNGTH)
670 918 FORMAT(F8.4,4F8.2//)
675 912 FORMAT(1HO,4X,4HMMAX,3X,5HMUMAX,3X,5HQUMAX,4X,4HMBAR)
680 919 FORMAT(4(5X,I3)///)
681 935 FORMAT(1HO,2X,6HQQSUM=,F12.5,2X,3HQQ=,I2,2X,3HQU=,
682&I2,2X,3HMU=,I2)
683 936 FORMAT(1HO,2X,7HFISUQU=,F12.5,2X,3HQQ=,I2,2X,3HQU=,
684&I2,2X,3HMU=,I2)
685 913 FORMAT(1HO,1X,1HI,5X,4HPHEE,6X,6HEFUNC)
686 937 FORMAT(1HO,2X,7HSECSUM=,F12.5,2X,3HQQ=,I2,2X,3HQU=,
687&I2,2X,3HMU=,I2)
690 980 FORMAT(9HDISCR=0.0)
693 932 FORMAT(1HO,2X,7HSMUSUM=,F12.5,2X,3HMU=,I2,2X,3HQU=,
694&I2,2X,2HM=,I2)
695 933 FORMAT(1HO,2X,5HQSUM=,F12.5,2X,3HMU=,I2,2X,3HQU=,
696&I2,2X,2HM=,I2)
697 934 FORMAT(1HO,2X,7HFIRSUM=,F12.5,2X,3HMU=,I2,2X,3HQU=,
698&I2,2X,2HM=,I2)
700 952 FORMAT(I3,2(1PE12.4))
705 END
710 SUBROUTINE TANHY(X,Y,Z)
715 RR=SQRT(ABS(X))
720 RS=RR*Y
725 Z=-RR*(EXP(RS)-EXP(-RS))/(EXP(RS)+EXP(-RS))
730 RETURN
735 END
740 SUBROUTINE TAN(X,Y,Z)
741 RT=SQRT(X)
742 RU=RT*Y
743 Z=RT*(SIN(RU)/COS(RU))
745 RETURN
746 END
747 SUBROUTINE ARG(TA,TB,TC,TD,TE,TF)
748 PI=3.141592
749 IF(TC)720,720,730
751 730 IF(TA)731,731,732
752 720 IF(TA)733,733,734
```

```
753 733 TF=TD
754 G0 T0 710
755 734 TF=0.
757 G0 T0 710
758 731 XI=TC*PI/TE
759 TF=(SIN(XI*(TB+1.0)*TD)-SIN(XI*TB*TD))/XI
760 G0 T0 710
761 732 JK=TA
762 XA=(-1.0)**JK
763 XB=TC*PI*TD/TE
764 XC=XB*TB
765 XD=XB*(TB+1.0)
766 XE=TC*PI/TE
767 XF=TA*PI/TD
768 IF(XE-XF)760,761,760
770 761 TF=TD*C0S(TA*TB*PI)/2.0
772 G0 T0 710
773 760 XG=XE/(XF*XF-XE*XE)
774 TF=XG*(SIN(XC)-XA*SIN(XD))
776 710 C0NTINUE
777 RETURN
778 END
779 SUBR0UTINE ARI(PHEE,WDTH,SMLEL,SMLW,XLNGTH,RET9,
780&MUMAX,QUMAX,MMAX,MBAR,MU1,NS,Q1MAX,FMUD,FQUD,X1)
781 INTEGER QU,QQ,QUMAX,QU2,Q1MAX
782 DIMENSI0N RET9(20,20,1),X1(20,20,1)
783 NN=1
784 1 D0 175 MU2=1,MUMAX
785 D0 176 QU2=1,QUMAX
786 PI=3.141592
787 FIRSUM=0.
788 D0 200 M=1,MMAX
790 FM=FL0AT(M-1)
791 AA=FM*PI/WDTH
792 DISCR=PHEE*PHEE-AA*AA
793 IF(DISCR)50,51,52
794 50 ART=SQRT(-DISCR)*XLNGTH
796 IF(ART-4.0)850,851,851
797 850 RR=SQRT(ABS(DISCR))
798 RS=RR*XLNGTH
799 RET=-RR*(EXP(RS)-EXP(-RS))/(EXP(RS)+EXP(-RS))
801 G0 T0 852
802 851 RET=-SQRT(ABS(DISCR))
803 852G0 T0300
804 51 ST0P
806 G0 T0 10
807 52 RT=SQRT(DISCR)
808 RU=RT*XLNGTH
809 RET=RT*(SIN(RU)/C0S(RU))
811 300 SMUSUM=0.
812 D0 220 MU=1,MUMAX
813 FMU=FL0AT(MU-1)
814 QSUM=0.
815 D0 210 QU=1,Q1MAX
```

```
816 FQU=FLØAT(QU)
817 FQU=FQU-1.0
818 IF(FQU)60,60,62
819 60 EPQU=1.0
821 GØ TØ 301
822 62 EPQU=2.
823 301 AB=FQU*PI/SMLW
824 DISCR2=PHEE*PHEE-AB*AB
826 IF(DISCR2)65,66,67
827 65 ARP=SQRT(-DISCR2)*SMLEL
828 IF(ARP-4.0)860,861,861
829 860 RR=SQRT(ABS(DISCR2))
830 RS=RR*SMLEL
832 RET2=-RR*(EXP(RS)-EXP(-RS))/(EXP(RS)+EXP(-RS))
833 GØ TØ 347
834 861 RET2=-SQRT(ABS(DISCR2))
836 GØ TØ 347
837 66 PRINT 980
838 10 STØP
839 67 RT=SQRT(DISCR2)
841 RU=RT*SMLEL
842 RET2=RT*(SIN(RU)/CØS(RU))
843 347 IF(FM)720,720,730
844 730 IF(FQU)731,731,732
846 720 IF(FQU)733,733,734
847 733 RET3=SMLW
848 GØ TØ 710
849 734 RET3=0.
851 GØ TØ 710
852 731 XI=FM*PI/WDTH
853 RET3=(SIN(XI*(FMU+1.0)*SMLW)-SIN(XI*FMU*SMLW))/XI
854 GØ TØ 710
856 732 JK=FQU
857 XA=(-1.0)**JK
858 XB=FM*PI*SMLW/WDTH
859 XC=XB*FMU
861 XD=XB*(FMU+1.)
862 XE=FM*PI/WDTH
863 XF=FQU*PI/SMLW
864 IF(XE-XF)760,761,760
866 761 RET3=SMLW*CØS(FMU*FQU*PI)/2.0
867 GØ TØ 710
868 760 XG=XE/(XF*XF-XE*XE)
869 RET3=XG*(SIN(XC)-XA*SIN(XD))
870 710 CØNTINUE
871 FQUD=FLØAT(QU2-1)
872 FMUD=FLØAT(MU2-1)
873 FMBAR=FLØAT(MBAR)
874 QSUM=QSUM+EPQU*RET2*RET3*RET9(QU,MU,MBAR)/SMLW
876 210 CØNTINUE
877 SMUSUM=SMUSUM+QSUM
878 220 CØNTINUE
879 IF(FM)70,70,71
```

```
881 70 EPM=1.
882 GØ TØ 303
883 71 EPM=2.0
884 303 IF(FM)920,920,930
886 930 IF(FQUD)931,931,932
887 920 IF(FQUD)933,933,934
888 933 RET8=SMLW
889 GØ TØ 910
891 934 RET8=0.
892 GØ TØ910
893 931 XI=FM*PI/WDTH
894 RET8=(SIN(XI*(FMUD+1.0)*SMLW)-SIN(XI*FMUD*SMLW))/XI
896 GØ TØ 910
897 932 JK=FQUD
898 XA=(-1.0)**JK
899 XB=FM*PI*SMLW/WDTH
901 XC=XB*FMUD
902 XD=XB*(FMUD+1.0)
903 XE=FM*PI/WDTH
904 XF=FQUD*PI/SMLW
906 IF(XE-XF)960,961,960
907 961 RET8=SMLW*CØS(FQUD*FMUD*PI)/2.0
908 GØ TØ 910
909 960 XG=XE/(XF*XF-XE*XE)
911 RET8=XG*(SIN(XC)-XA*SIN(XD))
912 910 CØNTINUE
913 FIRSUM=FIRSUM-EPM*SMUSUM*RET8/(RET*WDTH)
914 200 CØNTINUE
915 955 FØRMAT(4F10.5,2I3)
916 X1(QU2,MU2,MBAR)=FIRSUM
918 176 CØNTINUE
919 175 CØNTINUE
920 IF(NN-NS)6,7,7
922 6 DØ 188 MU2=1,MUMAX
923 DØ 182 QU2=1,QUMAX
924 RET9(QU2,MU2,MBAR)=X1(QU2,MU2,MBAR)
925 182 CØNTINUE
926 188 CØNTINUE
927 NN=NN+1
928 GØ TØ1
929 7 DØ 183 MU2=1,MUMAX
930 DØ 184 QU2=1,QUMAX
931 A=A
933 184 CØNTINUE
934 183 CØNTINUE
935 980 FØRMAT(2HNØ)
938 956 FØRMAT(F10.5,2I3)
940 RETURN
950 END
```

```
SSVEL2     13:29  RØCKET

50C    PRESSURE DISTRIBUTIØN-CØMPARTMENT SIDE
55 INTEGER QU,QQ,QUMAX,QU2,Q1MAX
56 DIMENSIØN RET9(20,20,1),X1(20,20,1)
70 10 PRINT 915
72 915 FØRMAT(1HO,2X,26HINPUT: PHEE,IC0N,NUMB,STEP)
73 INPUT,PHEE1,IC0N,NUMB,STEP
75 PRINT 916
76 916 FØRMAT(1HO,2X,19HINPUT: MU1,NS,Q1MAX)
77 INPUT,MU1,NS,Q1MAX
78 PRINT 917
79 917 FØRMAT(1HO,2X,20HINPUT: Y,STEP,SMLEL1)
80 INPUT,Y,STEP,SMLEL1
81 PRINT 918
82 918 FØRMAT(1HO,2X,51HINPUT: MUMAX,QUMAX,MMAX,MBAR,WDTH,
83&SMLW,SMLEL,XLNGTH)
84 INPUT,MUMAX,QUMAX,MMAX,MBAR,WDTH,SMLW,SMLEL,XLNGTH
87 PHEE=PHEE1/WDTH
88 PI=3.141592
89 15 DØ 170 MU2=1,MUMAX
90 DØ 171 QU2=1,QUMAX
92 FMBAR=FL0AT(MBAR)
93 PI=3.141592
94 RET9(QU2,MU2,MBAR)=0.
95 171 CØNTINUE
96 170 CØNTINUE
97 DØ 172 MU2=1,MUMAX
98 QU2=1
99 FMU2=FL0AT(MU2-1)
101 FQU2=FL0AT(QU2-1)
102 IF(FMBAR)21,21,22
103 22 IF(FQU2)31,31,32
104 21 IF(FQU2)33,33,34
105 33 RET9(QU2,MU2,MBAR)=SMLW
107 G0 T0 11
108 34 RET9(QU2,MU2,MBAR)=0.0
109 G0 T0 11
111 31 XI=FMBAR*PI/WDTH
112 RET9(QU2,MU2,MBAR)=(SIN(XI*(FMU2+1.0)*SMLW)
113&-SIN(XI*FMU2*SMLW))/XI
114 G0 T0 11
115 32 JK=FQU2
116 XA=(-1.0)**JK
117 XF=FQU2*PI/SMLW
118 XB=FMBAR*PI*SMLW/WDTH
119 XC=XB*FMU2
121 XD=XB*(FMU2+1.0)
122 XE=FMBAR*PI/WDTH
123 IF(XE-XF)58,59,58
124 59 RET9(QU2,MU2,MBAR)=SMLW*C0S(FMU2*FQU2*PI)/2.0
```

```
125 GØ TØ 11
126 58 XG=XE/(XF*XF-XE*XE)
128 RET9(QU2,MU2,MBAR)=XG*(SIN(XC)-XA*SIN(XD))
129 11 CØNTINUE
131 173 CØNTINUE
132 172 CØNTINUE
133 CALL ARI(PHEE,WDTH,SMLEL,SMLW,XLNGTH,RET9,
134&MUMAX,QUMAX,MMAX,MBAR,MU1,NS,Q1MAX,FMUD,FQUD,X1)
135 PI=3.141592
136 WDTH=20.
140 MU=MU1
150 FMU=FLØAT(MU-1)
152 DUM=(FMU+1.0)*SMLW
160 19 QUSUM=0.
170 DØ 210 QU=1,QUMAX
180 FQU=FLØAT(QU-1)
190 IF(FQU)40,41,40
200 41 EPQU=1.0
210 GØ TØ 50
220 40 EPQU=2.0
230 50 AB=FQU*PI/SMLW
240 DISCR=PHEE*PHEE-AB*AB
250 IF (DISCR)42,43,44
259 43 STØP
260 42 AR1=SQRT(-DISCR)*SMLEL1
261 AR4=SQRT(-DISCR)*SMLEL
262 AR2=(EXP(AR1)-EXP(-AR1))/2.0
263 AR3=(EXP(AR4)+EXP(-AR4))/2.0
270 AT=-SQRT(-DISCR)*AR2
280 AU=AR3
290 GØ TØ 60
300 44 AT=SQRT(DISCR)*SIN(SQRT(DISCR)*SMLEL1)
310 AU=CØS(SQRT(DISCR)*SMLEL)
319 FQP=0.0
320 60 CALL ARG(FQP,FMU,FMBAR,SMLW,WDTH,RET)
330 AV=CØS(FQU*PI*(Y-FMU*SMLW)/SMLW)
340 QU1=EPQU*X1(QU,MU,MBAR)*AV/SMLW
350 QUSUM=QUSUM+QU1
360 210 CØNTINUE
375 PRINT 900,Y,QUSUM
380 IF(Y-DUM)70,71,71
390 71 Y=DUM
400 GØ TØ 200
410 70 Y=Y+.1
411 GØ TØ 19
430 200 CØNTINUE
440 900 FØRMAT(1HO,2X,2HY=,F6.3,3X,4HPBS=,F10.4)
450 GØ TØ 10
460 END
710 SUBRØUTINE TANHY(X,Y,Z)
715 RR=SQRT(ABS(X))
```

```
720 RS=RR*Y
725 Z=-RR*(EXP(RS)-EXP(-RS))/(EXP(RS)+EXP(-RS))
730 RETURN
735 END
740 SUBRØUTINE TAN(X,Y,Z)
741 RT=SQRT(X)
742 RU=RT*Y
743 Z=RT*(SIN(RU)/CØS(RU))
745 RETURN
746 END
747 SUBRØUTINE ARG(TA,TB,TC,TD,TE,TF)
748 PI=3.141592
749 IF(TC)720,720,730
751 730 IF(TA)731,731,732
752 720 IF(TA)733,733,734
753 733 TF=TD
754 GØ TØ 710
755 734 TF=0.
757 GØ TØ 710
758 731 XI=TC*PI/TE
759 TF=(SIN(XI*(TB+1.0)*TD)-SIN(XI*TB*TD))/XI
760 GØ TØ 710
761 732 JK=TA
762 XA=(-1.0)**JK
763 XB=TC*PI*TD/TE
764 XC=XB*TB
765 XD=XB*(TB+1.0)
766 XE=TC*PI/TE
767 XF=TA*PI/TD
768 IF(XE-XF)760,761,760
770 761 TF=TD*CØS(TA*TB*PI)/2.0
772 GØ TØ 710
773 760 XG=XE/(XF*XF-XE*XE)
774 TF=XG*(SIN(XC)-XA*SIN(XD))
776 710 CØNTINUE
777 RETURN
778 END
779 SUBRØUTINE ARI(PHEE,WDTH,SMLEL,SMLW,XLNGTH,RET9,
780&MUMAX,QUMAX,MMAX,MBAR,MU1,NS,Q1MAX,FMUD,FQUD,X1)
781 INTEGER QU,QQ,QUMAX,QU2,Q1MAX
782 DIMENSIØN RET9(20,20,1),X1(20,20,1)
783 NN=1
784 1 DØ 175 MU2=1,MUMAX
785 DØ 176 QU2=1,QUMAX
786 PI=3.141592
787 FIRSUM=0.
788 DØ 200 M=1,MMAX
790 FM=FLØAT(M-1)
791 AA=FM*PI/WDTH
792 DISCR=PHEE*PHEE-AA*AA
793 IF(DISCR)50,51,52
```

```
794 50 ART=SQRT(-DISCR)*XLNGTH
796 IF(ART-4.0)850,851,851
797 850 RR=SQRT(ABS(DISCR))
798 RS=RR*XLNGTH
799 RET=-RR*(EXP(RS)-EXP(-RS))/(EXP(RS)+EXP(-RS))
801 GØ TØ 852
802 851 RET=-SQRT(ABS(DISCR))
803 852GØ TØ300
804 51 STØP
806 GØ TØ 10
807 52 RT=SQRT(DISCR)
808 RU=RT*XLNGTH
809 RET=RT*(SIN(RU)/CØS(RU))
811 300 SMUSUM=0.
812 DØ 220 MU=1,MUMAX
813 FMU=FLØAT(MU-1)
814 QSUM=0.
815 DØ 210 QU=1,Q1MAX
816 FQU=FLØAT(QU)
817 FQU=FQU-1.0
818 IF(FQU)60,60,62
819 60 EPQU=1.0
821 GØ TØ 301
822 62 EPQU=2.
823 301 AB=FQU*PI/SMLW
824 DISCR2=PHEE*PHEE-AB*AB
826 IF(DISCR2)65,66,67
827 65 ARP=SQRT(-DISCR2)*SMLEL
828 IF(ARP-4.0)860,861,861
829 860 RR=SQRT(ABS(DISCR2))
830 RS=RR*SMLEL
832 RET2=-RR*(EXP(RS)-EXP(-RS))/(EXP(RS)+EXP(-RS))
833 GØ TØ 347
834 861 RET2=-SQRT(ABS(DISCR2))
836 GØ TØ 347
837 66 PRINT 980
838 10 STØP
839 67 RT=SQRT(DISCR2)
841 RU=RT*SMLEL
842 RET2=RT*(SIN(RU)/CØS(RU))
843 347 IF(FM)720,720,730
844 730 IF(FQU)731,731,732
846 720 IF(FQU)733,733,734
847 733 RET3=SMLW
848 GØ TØ 710
849 734 RET3=0.
851 GØ TØ 710
852 731 XI=FM*PI/WDTH
853 RET3=(SIN(XI*(FMU+1.0)*SMLW)-SIN(XI*FMU*SMLW))/XI
```

```
854 GØ TØ 710
856 732 JK=FQU
857 XA=(-1.0)**JK
858 XB=FM*PI*SMLW/WDTH
859 XC=XB*FMU
861 XD=XB*(FMU+1.)
862 XE=FM*PI/WDTH
863 XF=FQU*PI/SMLW
864 IF(XE-XF)760,761,760
866 761 RET3=SMLW*CØS(FMU*FQU*PI)/2.0
867 GØ TØ 710
868 760 XG=XE/(XF*XF-XE*XE)
869 RET3=XG*(SIN(XC)-XA*SIN(XD))
870 710 CØNTINUE
871 FQUD=FLØAT(QU2-1)
872 FMUD=FLØAT(MU2-1)
873 FMBAR=FLØAT(MBAR)
874 QSUM=QSUM+EPQU*RET2*RET3*RET9(QU,MU,MBAR)/SMLW
876 210 CØNTINUE
877 SMUSUM=SMUSUM+QSUM
878 220 CØNTINUE
879 IF(FM)70,70,71
881 70 EPM=1.
882 GØ TØ 303
883 71 EPM=2.0
884 303 IF(FM)920,920,930
886 930 IF(FQUD)931,931,932
887 920 IF(FQUD)933,933,934
888 933 RET8=SMLW
889 GØ TØ 910
891 934 RET8=0.
892 GØ TØ910
893 931 XI=FM*PI/WDTH
894 RET8=(SIN(XI*(FMUD+1.0)*SMLW)-SIN(XI*FMUD*SMLW))/XI
896 GØ TØ 910
897 932 JK=FQUD
898 XA=(-1.0)**JK
899 XB=FM*PI*SMLW/WDTH
901 XC=XB*FMUD
902 XD=XB*(FMUD+1.0)
903 XE=FM*PI/WDTH
904 XF=FQUD*PI/SMLW
906 IF(XE-XF)960,961,960
907 961 RET8=SMLW*CØS(FQUD*FMUD*PI)/2.0
908 GØ TØ 910
909 960 XG=XE/(XF*XF-XE*XE)
911 RET8=XG*(SIN(XC)-XA*SIN(XD))
912 910 CØNTINUE
```

```
913 FIRSUM=FIRSUM-EPM*SMUSUM*RET8/(RET*WDTH)
914 200 CØNTINUE
915 955 FØRMAT(4F10.5,2I3)
916 X1(QU2,MU2,MBAR)=FIRSUM
918 176 CØNTINUE
919 175 CØNTINUE
920 IF(NN-NS)6,7,7
922 6 DØ 188 MU2=1,MUMAX
923 DØ 182 QU2=1,QUMAX
924 RET9(QU2,MU2,MBAR)=X1(QU2,MU2,MBAR)
925 182 CØNTINUE
926 188 CØNTINUE
927 NN=NN+1
928 GØ TØ1
929 7 DØ 183 MU2=1,MUMAX
930 DØ 184 QU2=1,QUMAX
931 A=A
933 184 CØNTINUE
934 183 CØNTINUE
935 980 FØRMAT(2HNØ)
938 956 FØRMAT(F10.5,2I3)
940 RETURN
950 END
```

```
SSBPD2     11:28  RØCKET

50C PRESSURE DISTRIBUTIØN-CHAMBER SIDE
55 INTEGER QU,QQ,QUMAX,QU2,Q1MAX
56 DIMENSIØN RET9(20,20,1),X1(20,20,1)
60 10 PRINT 915
61 Y=0.
65 915 FØRMAT(1HO,2X,26HINPUT: PHEE,ICØN,NUMB,STEP)
70 INPUT,PHEE1,ICØN,NUMB,STEP
71 PRINT 917
72 917 FØRMAT(1HO,2X,19HINPUT: MU1,NS,Q1MAX)
73 INPUT,MU1,NS,Q1MAX
75 IF(ICØN)20,20,30
76 30 PRINT 916
77 916 FØRMAT(1HO,2X,51HINPUT:MUMAX,QUMAX,MMAX,MBAR,WDTH,
78&SMLW,SMLEL,XLNGTH )
79 INPUT,MUMAX,QUMAX,MMAX,MBAR,WDTH,SMLW,SMLEL,XLNGTH
81 20 PRINT 910
82 N=1
83 PRINT 911
84 PRINT 918,PHEE1,WDTH,SMLW,SMLEL,XLNGTH
85 PRINT 912
86 PRINT 919,MMAX,MUMAX,QUMAX,MBAR
87 PHEE=PHEE1/WDTH
89 15 DØ 170 MU2=1,MUMAX
90 DØ 171 QU2=1,QUMAX
92 FMBAR=FLØAT(MBAR)
93 PI=3.141592
94 RET9(QU2,MU2,MBAR)=0.
95 171 CØNTINUE
96 170 CØNTINUE
97 DØ 172 MU2=1,MUMAX
98 QU2=1
99 FMU2=FLØAT(MU2-1)
101 FQU2=FLØAT(QU2-1)
102 IF(FMBAR)21,21,22
103 22 IF(FQU2)31,31,32
104 21 IF(FQU2)33,33,34
105 33 RET9(QU2,MU2,MBAR)=SMLW
107 GØ TØ 11
108 34 RET9(QU2,MU2,MBAR)=0.0
109 GØ TØ 11
110 PRINT 911
111 31 XI=FMBAR*PI/WDTH
112 RET9(QU2,MU2,MBAR)=(SIN(XI*(FMU2+1.0)*SMLW)
113&-SIN(XI*FMU2*SMLW))/XI
114 GØ TØ 11
115 32 JK=FQU2
116 XA=(-1.0)**JK
117 XF=FQU2*PI/SMLW
118 XB=FMBAR*PI*SMLW/WDTH
```

```
119 XC=XB*FMU2
120 PRINT 912
121 XD=XB*(FMU2+1.0)
122 XE=FMBAR*PI/WDTH
123 IF(XE-XF)58,59,58
124 59 RET9(QU2,MU2,MBAR)=SMLW*C0S(FMU2*FQU2*PI)/2.0
125 G0 T0 11
126 58 XG=XE/(XF*XF-XE*XE)
128 RET9(QU2,MU2,MBAR)=XG*(SIN(XC)-XA*SIN(XD))
129 11 C0NTINUE
131 173 C0NTINUE
132 172 C0NTINUE
133 CALL ARI(PHEE,WDTH,SMLEL,SMLW,XLNGTH,RET9,
134&MUMAX,QUMAX,MMAX,MBAR,MU1,NS,Q1MAX,FMUD,FQUD,X1)
135 PI=3.141592
140 FIRSUM=0.
145 D0 200 M=1,MMAX
150 FM=FL0AT(M-1)
155 AA=FM*PI/WDTH
160 DISCR=PHEE*PHEE-AA*AA
165 IF(DISCR)50,51,52
170 50 ART=SQRT(-DISCR)*XLNGTH
175 IF(ART-4.)850,851,851
180 850 CALL TANHY(DISCR,XLNGTH,RET)
185 G0 T0 852
190 851 RET=-SQRT(ABS(DISCR))
195 852 G0 T0 300
200 51 PRINT 980
205 G0 T0 10
210 52 CALL TAN(DISCR,XLNGTH,RET)
215 300 QSUM=0.
220 D0 210 QU=1,QUMAX
225 FQU=FL0AT(QU-1)
230 IF(FQU)60,60,62
235 60 EPQU=1.0
240 G0 T0 301
245 62 EPQU=2.0
250 301 AB=FQU*PI/SMLW
255 DISCR2=PHEE*PHEE-AB*AB
260 IF(DISCR2)65,66,67
265 65 ARP=SQRT(-DISCR2)*SMLEL
270 IF(ARP-4.)860,861,861
275 860 CALL TANHY(DISCR2,SMLEL,RET2)
280 G0 T0 347
285 861 RET2=-SQRT(ABS(DISCR2))
286 G0 T0 347
290 66 PRINT 980
295 G0 T0 10
300 67 CALL TAN(DISCR2,SMLEL,RET2)
305 347 SMUSUM=0.0
310 302 D0 220 MU=1,MUMAX
```

```
315 FMU=FLØAT(MU-1)
325 CALL ARG(FQU,FMU,FM,SMLW,WDTH,RET3)
330 FMBAR=FLØAT(MBAR)
334 FQP=0.0
343 SMUSUM=SMUSUM+EPQU*RET2*RET3*X1(QU,MU,MBAR)/SMLW
345 220 CØNTINUE
355 QSUM=QSUM+SMUSUM
360 210 CØNTINUE
365 IF(FM)70,70,71
370 70 EPM=1.0
375 GØ TØ 303
380 71 EPM=2.0
385 303 FIRSUM=FIRSUM+EPM*QSUM*CØS(FM*PI*Y/WDTH)/(RET*WDTH)
388 200 CØNTINUE
392 PRINT 994,PHEE1,Y,FIRSUM
393 994 FØRMAT(1HØ,2X,5HPHEE=,F10.5,3X,2HY=,F5.2,3X,3HPC=,F12.5)
394 IF(Y-10.)90,91,91
395 90 Y=Y+.1
396 GØ TØ 15
397 91 GØ TØ 10
660 910 FØRMAT(35HINITIAL VALUES FØR THIS CALCULATIØN//)
665 911 FØRMAT(1HØ,3X,4HPHEE,4X,4HWDTH,4X,5HSMLW ,3X,5HSMLEL,
666&2X,6HXLNGTH)
670 918 FØRMAT(F8.4,4F8.2//)
675 912 FØRMAT(1HØ,4X,4HMMAX,3X,5HMUMAX,3X,5HQUMAX,4X,4HMBAR)
680 919 FØRMAT(4(5X,I3)///)
690 980 FØRMAT(9HDISCR=0.0)
700 952 FØRMAT(I3,2(1PE12.4))
705 END
710 SUBRØUTINE TANHY(X,Y,Z)
715 RR=SQRT(ABS(X))
720 RS=RR*Y
725 Z=-RR*(EXP(RS)-EXP(-RS))/(EXP(RS)+EXP(-RS))
730 RETURN
735 END
740 SUBRØUTINE TAN(X,Y,Z)
741 RT=SQRT(X)
742 RU=RT*Y
743 Z=RT*(SIN(RU)/CØS(RU))
745 RETURN
746 END
747 SUBRØUTINE ARG(TA,TB,TC,TD,TE,TF)
748 PI=3.141592
749 IF(TC)720,720,730
751 730 IF(TA)731,731,732
752 720 IF(TA)733,733,734
753 733 TF=TD
754 GØ TØ 710
755 734 TF=0.
757 GØ TØ 710
758 731 XI=TC*PI/TE
```

```
759 TF=(SIN(XI*(TB+1.0)*TD)-SIN(XI*TB*TD))/XI
760 GØ TØ 710
761 732 JK=TA
762 XA=(-1.0)**JK
763 XB=TC*PI*TD/TE
764 XC=XB*TB
765 XD=XB*(TB+1.0)
766 XE=TC*PI/TE
767 XF=TA*PI/TD
768 IF(XE-XF)760,761,760
770 761 TF=TD*CØS(TA*TB*PI)/2.0
772 GØ TØ 710
773 760 XG=XE/(XF*XF-XE*XE)
774 TF=XG*(SIN(XC)-XA*SIN(XD))
776 710 CØNTINUE
777 RETURN
778 END
779 SUBRØUTINE ARI(PHEE,WDTH,SMLEL,SMLW,XLNGTH,RET9,
780&MUMAX,QUMAX,MMAX,MBAR,MU1,NS,Q1MAX,FMUD,FQUD,X1)
781 INTEGER QU,QQ,QUMAX,QU2,Q1MAX
782 DIMENSIØN RET9(20,20,1),X1(20,20,1)
783 NN=1
784 1 DØ 175 MU2=1,MUMAX
785 DØ 176 QU2=1,QUMAX
786 PI=3.141592
787 FIRSUM=0.
788 DØ 200 M=1,MMAX
790 FM=FLØAT(M-1)
791 AA=FM*PI/WDTH
792 DISCR=PHEE*PHEE-AA*AA
793 IF(DISCR)50,51,52
794 50 ART=SQRT(-DISCR)*XLNGTH
796 IF(ART-4.0)850,851,851
797 850 RR=SQRT(ABS(DISCR))
798 RS=RR*XLNGTH
799 RET=-RR*(EXP(RS)-EXP(-RS))/(EXP(RS)+EXP(-RS))
801 GØ TØ 852
802 851 RET=-SQRT(ABS(DISCR))
803 852GØ TØ300
804 51 STØP
806 GØ TØ 10
807 52 RT=SQRT(DISCR)
808 RU=RT*XLNGTH
809 RET=RT*(SIN(RU)/CØS(RU))
811 300 SMUSUM=0.
812 DØ 220 MU=1,MUMAX
813 FMU=FLØAT(MU-1)
814 QSUM=0.
815 DØ 210 QU=1,Q1MAX
816 FQU=FLØAT(QU)
817 FQU=FQU-1.0
```

```
818 IF(FQU)60,60,62
819 60 EPQU=1.0
821 GØ TØ 301
822 62 EPQU=2.
823 301 AB=FQU*PI/SMLW
824 DISCR2=PHEE*PHEE-AB*AB
826 IF(DISCR2)65,66,67
827 65 ARP=SQRT(-DISCR2)*SMLEL
828 IF(ARP-4.0)860,861,861
829 860 RR=SQRT(ABS(DISCR2))
830 RS=RR*SMLEL
832 RET2=-RR*(EXP(RS)-EXP(-RS))/(EXP(RS)+EXP(-RS))
833 GØ TØ 347
834 861 RET2=-SQRT(ABS(DISCR2))
836 GØ TØ 347
837 66 PRINT 980
838 10 STØP
839 67 RT=SQRT(DISCR2)
841 RU=RT*SMLEL
842 RET2=RT*(SIN(RU)/CØS(RU))
843 347 IF(FM)720,720,730
844 730 IF(FQU)731,731,732
846 720 IF(FQU)733,733,734
847 733 RET3=SMLW
848 GØ TØ 710
849 734 RET3=0.
851 GØ TØ 710
852 731 XI=FM*PI/WDTH
853 RET3=(SIN(XI*(FMU+1.0)*SMLW)-SIN(XI*FMU*SMLW))/XI
854 GØ TØ 710
856 732 JK=FQU
857 XA=(-1.0)**JK
858 XB=FM*PI*SMLW/WDTH
859 XC=XB*FMU
861 XD=XB*(FMU+1.)
862 XE=FM*PI/WDTH
863 XF=FQU*PI/SMLW
864 IF(XE-XF)760,761,760
866 761 RET3=SMLW*CØS(FMU*FQU*PI)/2.0
867 GØ TØ 710
868 760 XG=XE/(XF*XF-XE*XE)
869 RET3=XG*(SIN(XC)-XA*SIN(XD))
870 710 CØNTINUE
871 FQUD=FLØAT(QU2-1)
872 FMUD=FLØAT(MU2-1)
873 FMBAR=FLØAT(MBAR)
874 QSUM=QSUM+EPQU*RET2*RET3*RET9(QU,MU,MBAR)/SMLW
876 210 CØNTINUE
877 SMUSUM=SMUSUM+QSUM
878 220 CØNTINUE
879 IF(FM)70,70,71
881 70 EPM=1.
```

```
882 GØ TØ 303
883 71 EPM=2.0
884 303 IF(FM)920,920,930
886 930 IF(FQUD)931,931,932
887 920 IF(FQUD)933,933,934
888 933 RET8=SMLW
889 GØ TØ 910
891 934 RET8=0.
892 GØ TØ910
893 931 XI=FM*PI/WDTH
894 RET8=(SIN(XI*(FMUD+1.0)*SMLW)-SIN(XI*FMUD*SMLW))/XI
896 GØ TØ 910
897 932 JK=FQUD
898 XA=(-1.0)**JK
899 XB=FM*PI*SMLW/WDTH
901 XC=XB*FMUD
902 XD=XB*(FMUD+1.0)
903 XE=FM*PI/WDTH
904 XF=FQUD*PI/SMLW
906 IF(XE-XF)960,961,960
907 961 RET8=SMLW*CØS(FQUD*FMUD*PI)/2.0
908 GØ TØ 910
909 960 XG=XE/(XF*XF-XE*XE)
911 RET8=XG*(SIN(XC)-XA*SIN(XD))
912 910 CØNTINUE
913 FIRSUM=FIRSUM-EPM*SMUSUM*RET8/(RET*WDTH)
914 200 CØNTINUE
915 955 FØRMAT(4F10.5,2I3)
916 X1(QU2,MU2,MBAR)=FIRSUM
918 176 CØNTINUE
919 175 CØNTINUE
920 IF(NN-NS)6,7,7
922 6 DØ 188 MU2=1,MUMAX
923 DØ 182 QU2=1,QUMAX
924 RET9(QU2,MU2,MBAR)=X1(QU2,MU2,MBAR)
925 182 CØNTINUE
926 188 CØNTINUE
927 NN=NN+1
928 GØ TØ1
929 7 DØ 183 MU2=1,MUMAX
930 DØ 184 QU2=1,QUMAX
931 A=A
933 184 CØNTINUE
934 183 CØNTINUE
935 980 FØRMAT(2HNØ)
938 956 FØRMAT(F10.5,2I3)
940 RETURN
950 END
```

```
SSMCE8     11:09  RØCKET

50C CHARACTERISTIC EQ'N FØR THE BAFFLE PRØBLEM(ACTIVE BØUNDARY)
51 CØMPLEX RET9,DISCR,PHEE,ART,RET,SMUSUM,QSUM,DISCR2,ARP,RET2,
52&DSUM,FISUQU,SECSUM,DISCR3,ARS,RET5,X1,TØSUM,PHEE2,PHEE3,FIRSUM,
53&PHEE1,ADA,REA,REB,YMA,YQ,REC,RED,REE,REF,FIND ,DFEFUN,YQ1,YQ2
55 INTEGER QU,QQ,QUMAX,QU2,Q1MAX
60 DIMENSIØN RET9(20,20,1),X1(20,20,1),TØSUM(3)
65 10 PRINT 915
67 915 FØRMAT(1HO,2X,26HINPUT: PHEE,ICØN,NUMB,STEP)
69 INPUT,PHEE1,ICØN,NUMB,STEP
71 IF(ICØN)20,20,30
73 30 PRINT 916
75 916 FØRMAT(1HO,2X,19HINPUT: MU1,NS,Q1MAX)
77 INPUT,MU1,NS,Q1MAX
79 PRINT 917
81 917 FØRMAT(1HO,2X,13HINPUT: YQ,YMA)
83 INPUT,YQ,YMA
85 PRINT 918
87 918 FØRMAT(1HO,2X,51HINPUT: MUMAX,QUMAX,MMAX,MBAR,WDTH,SMLW,
88&SMLEL,XLNGTH)
90 INPUT,MUMAX, QUMAX,MMAX,MBAR,WDTH,SMLW,SMLEL,XLNGTH
110 PHEE=PHEE1/WDTH
120 20 N=1
121 PRINT 913
146 15 DØ 169 JJ=1,3
147 FJJ=FLØAT(JJ-1)
148 FIND=CMPLX(.000001,.000001)
149 YQ=YQ+FJJ*FIND
155 DØ 170 MU2=1,MUMAX
160 DØ 171 QU2=1,QUMAX
165 FMBAR=FLØAT(MBAR)
170 PI=3.141592
175 RET9(QU2,MU2,MBAR)=CMPLX(0.,0.)
180 171 CØNTINUE
185 170 CØNTINUE
190 DØ 172 MU2=1,MUMAX
195 QU2=1
200 FMU2=FLØAT(MU2-1)
205 FQU2=FLØAT(QU2-1)
210 IF(FMBAR)21,21,22
215 22 IF(FQU2)31,31,32
220 21 IF(FQU2)33,33,34
225 33 RET9(QU2,MU2,MBAR)=SMLW
230 GØ TØ 11
235 34 RET9(QU2,MU2,MBAR)=0.0
240 GØ TØ 11
250 31 XI=FMBAR*PI/WDTH
255 RET9(QU2,MU2,MBAR)=(SIN(XI*(FMU2+1.0)*SMLW)
260&-SIN(XI*FMU2*SMLW))/XI
```

```
265 GØ TØ 11
270 32 JK=FQU2
275 XA=(-1.0)**JK
280 XF=FQU2*PI/SMLW
285 XB=FMBAR*PI*SMLW/WDTH
290 XC=XB*FMU2
300 XD=XB*(FMU2+1.0)
305 XE=FMBAR*PI/WDTH
310 IF(XE-XF)58,59,58
315 59 RET9(QU2,MU2,MBAR)=SMLW*CØS(FMU2*FQU2*PI)/2.0
320 GØ TØ 11
325 58 XG=XE/(XF*XF-XE*XE)
330 RET9(QU2,MU2,MBAR)=XG*(SIN(XC)-XA*SIN(XD))
335 11 CØNTINUE
340 173 CØNTINUE
345 172 CØNTINUE
350 CALL ARI(PHEE,WDTH,SMLEL,SMLW,XLNGTH,RET9,YMA,YQ,
355&MUMAX,QUMAX,MMAX,MBAR,MU1,NS,Q1MAX,FMUD,FQUD,X1)
360 PI=3.141592
365 FIRSUM=CMPLX(0.,0.)
370 DØ 200 M=1,MMAX
375 FM=FLØAT(M-1)
380 AA=FM*PI/WDTH
385 DISCR=PHEE*PHEE-AA*AA
390 IF(CABS(DISCR))50,51,52
395 50 ART=CSQRT(-DISCR)*XLNGTH
420 852 GØ TØ 300
425 51 PRINT 980
430 GØ TØ 10
435 52 CALL TAN(DISCR,XLNGTH,RET)
436 ADA=CMPLX(0.,1.)
437 REA=RET-ADA*PHEE*YMA
438 REB=1.0+ADA*PHEE*YMA*RET/(CSQRT(DISCR)*CSQRT(DISCR))
439 RET=REA/REB
440 300 SMUSUM=CMPLX(0.,0.)
445 DØ 220 MU=1,MUMAX
450 FMU=FLØAT(MU-1)
455 QSUM=CMPLX(0.,0.)
465 DØ 210 QU=1,QUMAX
470 FQU=FLØAT(QU-1)
475 IF(FQU)60,60,62
480 60 EPQU=1.0
485 GØ TØ 301
490 62 EPQU=2.0
495 301 AB=FQU*PI/SMLW
500 DISCR2=PHEE*PHEE-AB*AB
505 IF(CABS(DISCR2))65,66,67
510 65 ARP=CSQRT(-DISCR2)
535 GØ TØ 347
540 66 PRINT 980
545 GØ TØ 10
```

```
550 67 CALL TAN(DISCR2,SMLEL,RET2)
551 REC=RET2-ADA*PHEE*YQ
552 RED=1.0+ADA*PHEE*YQ*RET2/(CSQRT(DISCR2)*CSQRT(DISCR2))
553 RET2=REC/RED
555 347 FMBAR=FLØAT(MBAR)
560 CALL ARG(FQU,FMU,FM,SMLW,WDTH,RET3)
565 FQR=0.0
570 FMUD=FMU
575 FQUD=FQU
580 QSUM=QSUM+EPQU*RET2*RET3*X1(QU,MU,MBAR)/SMLW
585
590 FMU1=FLØAT(MU1-1)
595 210 CØNTINUE
600 IF(FMU-FMU1)4,5,4
605 5 DSUM=QSUM
610 4 SMUSUM=SMUSUM+QSUM
615 220 CØNTINUE
620 IF(FM)70,70,71
625 70 EPM=1.0
630 GØ TØ 303
635 71 EPM=2.0
640 303 FIRSUM=FIRSUM+SMUSUM*SMUSUM*EPM/(RET*WDTH)
645 200 CØNTINUE
650 SECSUM=CMPLX(0.,0.)
655 DØ 230 MU=1,MUMAX
665 FMU=FLØAT(MU-1)
670 FISUQU=CMPLX(0.,0.)
675 DØ 240 QU=1,QUMAX
680 FQU=FLØAT(QU-1)
685 IF(FQU)80,80,81
690 80 EPQU=1.0
695 GØ TØ 500
700 81 EPQU=2.0
705 500 AC=FQU*PI/SMLW
710 DISCR3=PHEE*PHEE-AC*AC
715 IF(CABS(DISCR3))90,91,92
720 90 ARS=CSQRT(-DISCR3)*SMLEL
750 91 PRINT 980
755 GØ TØ 10
760 92 CALL TAN(DISCR3,SMLEL,RET5)
761 REE=RET5-ADA*PHEE*YQ
762 REF=1.0+ADA*PHEE*YQ*RET5/(CSQRT(DISCR3)*CSQRT(DISCR3))
763 RET5=REE/REF
765 410 FQP=0.0
770 FMUD=FMU
775 FQUD=FQU
780 FISUQU=FISUQU+RET5*X1(QU,MU,MBAR)*X1(QU,MU,MBAR)*
785&EPQU/SMLW
790 240 CØNTINUE
795 SECSUM=SECSUM+FISUQU
796 230 CØNTINUE
```

```
800 953 FØRMAT(F12.6)
805 TØSUM(JJ)=FIRSUM+SECSUM
806 169 CØNTINUE
807 YQ2=YQ-FIND
808 DFEFUN=(TØSUM(3)-TØSUM(1))/(2.0*FIND)
809 YQ=YQ2-TØSUM(2)/DFEFUN
810 YQ1=YQ
815 PRINT 952,N,YQ1,TØSUM(2)
816 DFEDUM=CABS(TØSUM(2))
817 IF(DFEDUM-.000001)976,976,969
820 969 IF(N-NUMB)975,975,976
825 975 N=N+1
830 YQ=YQ-FIND
835 GØ TØ 15
840 976 GØ TØ 10
895 913 FØRMAT(1HO,1X,1HI,4X,6HR-PHEE,5X,6HI-PHEE
896&,6X,8HR-FEFUNC,6X,8HI-FEFUNC)
910 980 FØRMAT(9HDISCR=0.0)
945 952 FØRMAT(I3,4F12.8)
950 END
985 SUBRØUTINE TAN(X,Y,Z)
986 CØMPLEX X,RT,RU,Z
990 RT=CSQRT(X)
995 RU=RT*Y
1000 Z=RT*(CSIN(RU)/CCØS(RU))
1005 RETURN
1010 END
1015 SUBRØUTINE ARG(TA,TB,TC,TD,TE,TF)
1020 PI=3.141592
1025 IF(TC)720,720,730
1030 730 IF(TA)731,731,732
1035 720 IF(TA)733,733,734
1040 733 TF=TD
1045 GØ TØ 710
1050 734 TF=0.
1055 GØ TØ 710
1060 731 XI=TC*PI/TE
1065 TF=(SIN(XI*(TB+1.0)*TD)-SIN(XI*TB*TD))/XI
1070 GØ TØ 710
1075 732 JK=TA
1080 XA=(-1.0)**JK
1085 XB=TC*PI*TD/TE
1090 XC=XB*TB
1095 XD=XB*(TB+1.0)
1100 XE=TC*PI/TE
1105 XF=TA*PI/TD
1110 IF(XE-XF)760,761,760
1115 761 TF=TD*CØS(TA*TB*PI)/2.0
1120 GØ TØ 710
1125 760 XG=XE/(XF*XF-XE*XE)
1130 TF=XG*(SIN(XC)-XA*SIN(XD))
```

```
1135 710 CØNTINUE
1140 RETURN
1145 END
1150 SUBRØUTINE ARI(PHEE,WDTH,SMLEL,SMLW,XLNGTH,RET9,YMA,YQ,
1155&MUMAX,QUMAX,MMAX,MBAR,MU1,NS,Q1MAX,FMUD,FQUD,X1)
1156 CØMPLEX FIRSUM,DISCR,ART,RR,RS,RET,RT,RU,SMUSUM,
1157&QSUM,DISCR2,ARP,RET2,RET9,X1,ADA,REA,REB,YMA,YQ,REC,RED
1160 INTEGER QU,QQ,QUMAX,QU2,Q1MAX
1165 DIMENSIØN RET9(20,20,1),X1(20,20,1)
1170 NN=1
1175 1 DØ 175 MU2=1,MUMAX
1180 DØ 176 QU2=1,QUMAX
1185 PI=3.141592
1190 FIRSUM=CMPLX(0.,0.)
1195 DØ 200 M=1,MMAX
1200 FM=FLØAT(M-1)
1205 AA=FM*PI/WDTH
1210 DISCR=PHEE*PHEE-AA*AA
1215 IF(CABS(DISCR))50,51,52
1220 50 ART=CSQRT(-DISCR)*XLNGTH
1250 851 RET=-CSQRT(-DISCR)
1255 852GØ TØ300
1260 51 STØP
1265 GØ TØ 10
1270 52 CALL TAN(DISCR,XLNGTH,RET)
1281 ADA=CMPLX(0.0,1.0)
1282 REA=RET-ADA*PHEE*YMA
1283 REB=1.0+ADA*PHEE*YMA*RET/(CSQRT(DISCR)*CSQRT(DISCR))
1284 RET=REA/REB
1285 300 SMUSUM=CMPLX(0.,0.)
1290 DØ 220 MU=1,MUMAX
1295 FMU=FLØAT(MU-1)
1300 QSUM=CMPLX(0.,0.)
1305 DØ 210 QU=1,Q1MAX
1310 FQU=FLØAT(QU)
1315 FQU=FQU-1.0
1320 IF(FQU)60,60,62
1325 60 EPQU=1.0
1330 GØ TØ 301
1335 62 EPQU=2.
1340 301 AB=FQU*PI/SMLW
1345 DISCR2=PHEE*PHEE-AB*AB
1350 IF(CABS(DISCR2))65,66,67
1355 65 ARP=CSQRT(-DISCR2)*SMLEL
1395 66 PRINT 980
1400 10 STØP
1405 67 CALL TAN(DISCR2,SMLEL,RET2)
1415 REC=RET2-ADA*PHEE*YQ
```

```
1416 RED=1.0+ADA*PHEE*YQ*RET2/(CSQRT(DISCR2)*CSQRT(DISCR2))
1417 RET2=REC/RED
1420 347 CALL ARG(FQU,FMU,FM,SMLW,WDTH,RET3)
1535 FQUD=FL0AT(QU2-1)
1540 FMUD=FL0AT(MU2-1)
1545 FMBAR=FL0AT(MBAR)
1550 QSUM=QSUM+EPQU*RET2*RET3*RET9(QU,MU,MBAR)/SMLW
1555 210 C0NTINUE
1560 SMUSUM=SMUSUM+QSUM
1565 220 C0NTINUE
1570 IF(FM)70,70,71
1575 70 EPM=1.
1580 G0 T0 303
1585 71 EPM=2.0
1590 303 CALL ARG(FQUD,FMUD,FM,SMLW,WDTH,RET8)
1600
1705 FIRSUM=FIRSUM-EPM*SMUSUM*RET8/(RET*WDTH)
1710 200 C0NTINUE
1720 X1(QU2,MU2,MBAR)=FIRSUM
1725 176 C0NTINUE
1730 175 C0NTINUE
1735 IF(NN-NS)6,7,7
1740 6 D0 188 MU2=1,MUMAX
1745 D0 182 QU2=1,QUMAX
1750 RET9(QU2,MU2,MBAR)=X1(QU2,MU2,MBAR)
1755 182 C0NTINUE
1760 188 C0NTINUE
1765 NN=NN+1
1770 G0 T01
1775 7 C0NTINUE
1800 980 F0RMAT(2HN0)
1810 RETURN
1815 END
```

APPENDIX D

DISTRIBUTION

Dr. R. J. Priem MS 500-204
NASA Lewis Research Center
21000 Brookpark Road
Cleveland, Ohio 44135 (4)

Normal T. Musial
NASA Lewis Research Center
21000 Brookpark Road
Cleveland, Ohio 44135

Library (2)
NASA Lewis Research Center
21000 Brookpark Road
Cleveland, Ohio 44135

Report Control Office
NASA Lewis Research Center
21000 Brookpark Road
Cleveland, Ohio 44135

NASA Representative (6)
NASA Scientific and Technical
Information Facility
P.O. Box 33
College Park, Maryland 20740

V. Agosta
Brooklyn Polytechnic Institute
Long Island Graduate Center
Route 110
Farmingdale, New York 11735

B. P. Breen
Dynamic Science, a Division of
Marshall Industries
1900 Walker Avenue
Monrovia, California 91016

Thomas J. Chew
AFRPL (RPRRC)
Edwards, California 93523

T. W. Christian
Chemical Propulsion Information
Agency
8621 Georgia Avenue
Silver Spring, Maryland 20910

Lt. W. Pritz
AFRPL (RPRRC)
Edwards, California 93523

R. M. Clayton
Jet Propulsion Laboratory
California Institute of Technology
4800 Oak Grove Drive
Pasadena, California 91103

E. W. Conrad MS 500-204
NASA Lewis Research Center
21000 Brookpark Road
Cleveland, Ohio 44135

Dr. E. K. Dabora
University of Connecticut
Aerospace Department
Storrs, Connecticut 06268

O. W. Dykema
Aerospace Corporation
P.O. Box 95085
Los Angeles, California 90045

G. W. Elverum
TRW Systems
1 Space Park
Redondo Beach, California 90278

R. Edse
Ohio State University
Dept. of Aeronautical and
Astronautical Engineering
Columbus, Ohio 43210

G. M. Faeth
The Pennsylvania State University
Mechanical Engineering Department
207 Mechanical Engineering Blvd.
University Park, Pa. 16802

G. D. Garrison
Pratt and Whitney Aircraft
Florida Research and Development Ctr.
P.O. Box 2691
West Palm Beach, Florida 33402

M. Gerstein
Dept. Mech. Engr.
University of Southern California
University Park
Los Angeles, California 90007

I. Glassman
Princeton University
James Forrestal Research Center
P.O. Box 710
Princeton, New Jersey 08540

Richard W. Maffner
Air Force Office of Scientific Research
1400 Wilson Blvd.
Arlington, Virginia 22209

D. Harrje
Princeton University
James Forrestal Research Center
P.O. Box 710
Princeton, New Jersey 08540

T. Inouye Code 4581
U.S. Naval Weapons Center
China Lake, California 93555

R. D. Jackel, 429
Office of Naval Research
Navy Department
Washington, D.C. 20360

R. B. Lawhead
Rocketdyne
A Division of North American Rockwell Corporation
6633 Canoga Avenue
Canoga Park, California 91304

R. S. Levine, Code RPL
NASA Headquarters
6th and Independence Ave., S.W.
Washington, D.C. 20546

Ted Male MS 500-209
NASA Lewis Research Center
21000 Brookpark Road
Cleveland, Ohio 44135

J. M. McBride
Aerojet-General Corporation
P.O. Box 15847
Sacramento, California 95809

E. W. Price, Code 608
U.S. Naval Weapons Center
China Lake, California 93555

P. D. McCormack
Dartmouth University
Hanover, New Hampshire 03755

C. E. Mitchell
Colorado State University
Fort Collins, Colorado 80521

P. S. Myers
University of Wisconsin
Mechanical Engineering Dept.
1513 University Avenue
Madison, Wisconsin 53705

J. A. Nestlerode
Rocketdyne
A Division of North American Rockwell Corporation
6633 Canoga Avenue
Canoga Park, California 91304

J. A. Nicholls
University of Michigan
Aerospace Engineering
Ann Arbor, Michigan 48104

James C. O'Hara
Tulane University
Dept. of Mechanical Engr.
New Orleans, La. 70118

A. K. Oppenhiem
University of California
Dept. of Aeronautical Sciences
6161 Etcheverry Hall
Berkeley, California 94720

J. R. Osborn
Purdue University
School of Mechanical Engr.
Lafayette, Indiana 47907

Dr. K. Ragland
University of Wisconsin
Mechanical Engineering Dept.
Madison, Wisconsin 53705

Dr. A. A. Ranger
Purdue University
School of Aeronautics, Astronautics
and Engineering Sciences
Lafayette, Indiana 47907

F. H. Reardon
Sacramento State College
School of Engineering
6000 J. Street
Sacramento, California 95819

B. A. Reese
Purdue University
School of Mechanical Engineering
Lafayette, Indiana 47907

R. J. Richmond R-Pand VE-PA
NASA George C. Marshall Space
Flight Center
Huntsville, Alabama 35812

J. H. Rupe
Jet Propulsion Laboratory
California Institute of Technology
4800 Oak Grove Drive
Pasadena, California 91103

Dr. R. F. Sawyer
University of California
Mechanical Engineering, Thermal
Systems
Berkeley, California 94720

K. Scheller
ARL (ARC)
Wright-Patterson AFB
Dayton, Ohio 45433

Roger A. Strehlow
University of Illinois
Aeronautical Engineering Dept.
Urbana, Illinois 61801

J. G. Thibadaux
NASA Manned Spacecraft Center
Houston, Texas 77058

Warren Brasher/EP2
Primary Propulsion Branch
NASA Manned Spacecraft Center
Houston, Texas 77058

T. P. Torda
Illinois Institute of Technology
Room 200 M.H.
3300 S. Federal Street
Chicago, Illinois 60616

T. Y. Toong
Massachusetts Institute of Technology
Department of Mechanical Engineering
Cambridge, Massachusetts 02139

Richard Weiss
AFRPL
Edwards, California 93523

W. W. Wharton AMSMI-RKL
U.S. Army Missile Command
Redstone Arsenal, Alabama 35808

F. A. Williams
University of California
Aerospace Engineering Dept.
P.O. Box 109
LaJolla, California 92038

L. M. Wood
Bell Aerosystems Company
P.O. Box 1
Mail Zone J-81
Buffalo, New York 14205

B. T. Zinn
Georgia Institute of Technology
Aerospace School
Atlanta, Georgia 30332

Unclassified

Security Classification

DOCUMENT CONTROL DATA - R & D

(Security classification of title, body of abstract and indexing annotation must be entered when the overall report is classified)

1. ORIGINATING ACTIVITY *(Corporate author)* Rocketdyne, a Division of North American Rockwell Corporation, 6633 Canoga Avenue, Canoga Park, California 91304	2a. REPORT SECURITY CLASSIFICATION Unclassified 2b. GROUP

3. REPORT TITLE

Analysis of the Acoustic Behavior of Baffled Combustion Chambers

4. DESCRIPTIVE NOTES *(Type of report and inclusive dates)*

Final Report

5. AUTHOR(S) *(First name, middle initial, last name)*

Carl L. Oberg, T. L. Wong, and R. A. Schmeltzer

6. REPORT DATE	7a. TOTAL NO. OF PAGES	7b. NO. OF REFS
30 January 1970	92	7

8a. CONTRACT OR GRANT NO.	9a. ORIGINATOR'S REPORT NUMBER(S)
NAS 3-11226	R-8076
b. PROJECT NO.	
c.	9b. OTHER REPORT NO(S) *(Any other numbers that may be assigned this report)*
d.	CR-72625

10. DISTRIBUTION STATEMENT

11. SUPPLEMENTARY NOTES	12. SPONSORING MILITARY ACTIVITY

13. ABSTRACT As a means of studying the effects of baffles on acoustic modes of combustion instability, analytical methods have been developed for calculating the wave motion in closed, baffled chambers with rigid or nonrigid boundaries. These methods encompass solving the wave equation for the baffled chamber by converting the differential equation and boundary conditions to an integral equation which, in turn, is solved by approximate means. A variational technique in combination with an iterated approximation was used to solve the integral equation. Numerical results were obtained for two-dimensional chambers containing one or several equal length and equally spaced baffles. The results show an essentially continuous pressure distribution along the baffle tips. Requirements for continuity of velocity and energy flux are automatically met with this method. Furthermore, the effects of a single baffle on the stability of a chamber with nonrigid walls, i.e., gain/loss-type boundary conditions, has been successfully analyzed for one particular two-dimensional geometry. Thus, the ability to generalize the method for nonzero boundary conditions has also been demonstrated. Finally, convergence of the iteration scheme has not been proved but very good numerical results were obtained and it is likely that adequate convergence can be achieved.

DD FORM 1 NOV 65 1473

Unclassified

Security Classification

14. KEY WORDS	LINK A		LINK B		LINK C	
	ROLE	WT	ROLE	WT	ROLE	WT
Baffled Chambers						
Nonrigid Boundaries						
Rigid Boundaries						
Variation-Iteration Technique						
Integral Formulation						